Final Report

Federal Agency to which the report is submitted	U. S. Department of Energy, Office of Fossil Energy National Energy Technology Laboratory
Nature of the Report	Final Report
Award Number	DE-FE0029020
Award Type	
Name, Title, Email Address, and Phone Number for the Prime Recipient	Heath Spidle, Research Engineer, heath.spidle@swri.org, 210-522-6717
Prime Recipient Name and Address	Southwest Research Institute 6220 Culebra Road, San Antonio, TX 78238-5166
Prime Recipient type	Not for profit organization
Project Title	**Smart Methane Emission Detection System Development**
Principal Investigator(s)	Prime: Heath Spidle - SwRI
Prime Recipient's DUNS number	00-793-6842
Date of the Report	18 Nov 2021
Period Covered by the Report	01 October 2016 – 30 September 2021
Reporting Frequency	Final
Signature of Principal Investigator:	Heath Spidle

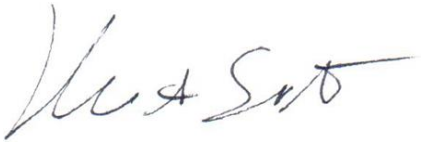

Table of Contents

LIST OF FIGURES

LIST OF TABLES

EXECUTIVE SUMMARY

Working with the U.S. Department of Energy's Office of Fossil Energy and the National Energy Technology Laboratory, Southwest Research Institute® (SwRI®) developed a system to identify methane leaks reliably, accurately, and autonomously at critical midstream sections of the natural gas distribution network in real-time for the purpose of mitigating methane emissions using Optical Gas Imaging (OGI) cameras. SwRI's Smart Leak Detection – Methane (SLED/M) adds a high degree of automation to the process of methane leak detection to minimize sources of human error, minimize response time to a leak event, and maximize midstream visibility. Furthermore, SwRI has been working towards integrating Quantitative OGI (QOGI) capabilities into this existing technology. By leveraging Deep Learning, SwRI now has the capability to estimate fugitive emission leak rates quickly and reliably, which allows operators to detect emissions, quantify leak rate, prioritize repairs, and validate the repairs in a single instrument. The next generation QOGI technology leverages the same cameras used in Leak Detection and Repair (LDAR) programs, with improvements in safety and speed for traditional quantification-based repairs, ultimately leading to less overhead cost for the operators.

The goals for this research were to develop two types of models with the following goals:

1. Run in real-time on the edge (≥ 12 Hz)
2. Classification: Achieve less than 5% false positive detection
3. Classification: Achieve ≥ 95% methane plume detection rate
4. Regression: achieve ≤ 10 standard cubic feet per hour (scfh) prediction > 70% of the time

In order to achieve these results, multiple infrared (IR) and other sensors were investigated in tandem with the midwave IR (MWIR) OGI to provide additional information to train the underlying models. Information on atmospheric conditions including humidity, temperature, pressure, and solar radiation was provided by a weather station. Several machine learning and deep learning architectures and methods, including looking at quantized classification networks and regressions networks, were explored. As further data was collected, curated, and labeled, it allowed for more refined regressive networks to be adequately trained, leading to better insight into the true flow rates being observed. An important valuable deliverable of this research effort was the development of an advanced network which underwent multiple iterations capable of giving a continuous output. The current network has a predicted mean average percentage error (MAPE) of 12.3% just outside our target goal of 10.00%, but an accuracy of 97.78% at ±50 scfh, well within the overall goal for the U.S. Department of Energy's (DOE) Office of Fossil Energy program. Upon closer inspection, it was observed that more than 10% of datapoints contributing to the MAPE predictions were the result of low flow rate predictions and are beyond the sensitivity of instrument measurement as a result of normal operational variation and noise. Figure 1 shows an example of both SLED-M detection network and subsequent concentration, with ground truth and predicted values in the upper portion of each frame.

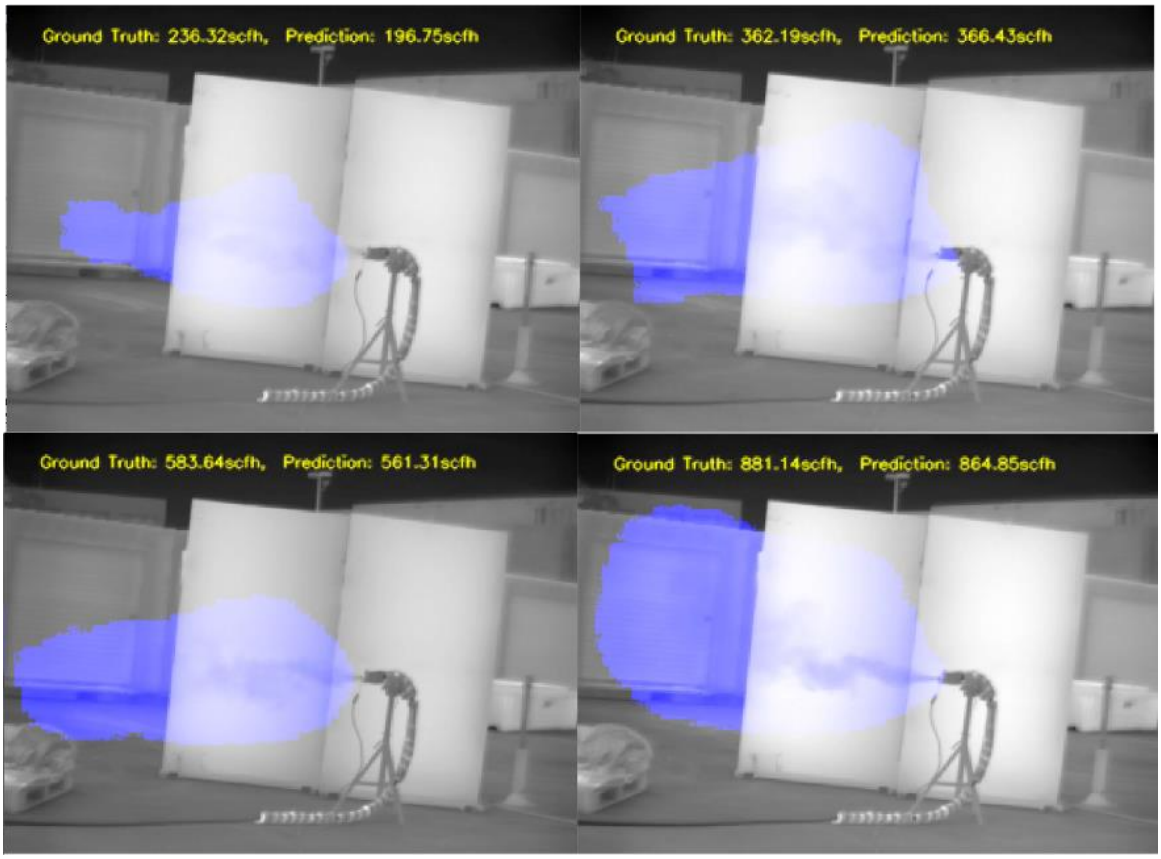

Figure 1. Detection and Quantification at Multiple Flowrates

1. INTRODUCTION

Compressor stations used to move natural gas in midstream applications are a significant contributor to methane emissions.[1] One of the largest sources of methane emissions in the midstream sector is fugitive emissions from compressors. According to this study, 50% of fugitive emissions are from major compressor equipment. This problem is most significant from reciprocating compressors where faulty seals are a key contributor to methane emissions.[2, 3] Fugitive emissions from such sources could go undetected for extended periods of time, resulting in the accumulation of significant emissions.

A key factor of site-level emissions, the "fat tail", found in which a small number of sites have a disproportionate amount of emissions, particularly within the midstream segment. As pointed out in Subramanian *et. al.*, 10% of emitting sites contributed to 50% of the overall emissions.[2] Thus, there is a significant need for a robust technology that could provide an early indication of an unexpected emission. Equally important, the technology needs to be able to account for biogenic versus anthrophonic sources of methane. One means of indirectly making this determination, is to leverage optical technologies that can autonomously pinpoint the source of such leaks.

According to a recent study by Stanford, only one methane detection technology out of ten tested was able to estimate leak rate to within a range of half to two times the actual rate only 53% of the time.[4] The other eight were only able to estimate to within an order of magnitude 74% of the time. All of these technologies rely on sniffer, or laser-based technologies. Per NSPS 40 CFR 60 (OOOOa), these technologies fall under the Method 21 rules, which requires the sensor to be within a few inches of the component in order to verify the fugitive emission, as well as to verify that the fugitive emission has been repaired. Under this same regulation OGI's are able to detect and verify fugitive emissions visibly, which can be done from much farther away and much faster. We believe if we could quantify emissions with an OGI, this could be a major disruption in the way inspections are carried out in today's oil and gas market.

In 2016, SwRI was awarded funding from a DOE – National Energy Technology Laboratory (NETL) grant to develop an autonomous, reliable, real-time methane leak detection technology, the Smart Methane Leak Detection System (SLED), which applies machine learning techniques to passive optical sensing modalities to mitigate emissions through early detection. The goals of this DOE program were as follows:

- Develop a system to identify methane leaks reliably, accurately, and autonomously at critical midstream sections of the natural gas distribution network in real-time for the purpose of mitigating methane emissions.
- Add a high degree of automation to the process of methane leak detection to minimize sources of human error, minimize response time to a leak event, and maximize midstream visibility.
- Assist in the quantification process by providing a means of collecting temporal and spatial image data of a leak event.
- Reduce operational costs of emissions detection technologies by significantly minimizing the need for operator involvement.
- Provide a solution that is scalable, cost-effective, and non-intrusive.

- Reduce methane emissions through early real-time, autonomous detection of methane leaks.

The project was conducted over four phases:

- Phase 1 developed the prototype methane detection system with integrated optical sensors and the embedded processing unit.
- Phase 2 implemented the prototype methane detection system developed under Phase 1 into deployed hardware and refined the unit performance.
- Phase 3 adapted the stationary algorithm developed in Phases 1 and 2 for deployment and operation on an Unmanned Aerial System (UAS)
- Phase 4 added quantification capabilities to the system

The output from this effort is SLED/M, an autonomous, real-time methane leak detection system which facilitates the early detection of emissions before they become a larger problem. Compressor station operators will be able to identify failing equipment in aging infrastructure and replace faulty components expediently, resulting in methane emissions being reduced significantly through early detection of non-compliant equipment. By adding the capability to estimate leak flow rates in conjunction with visual inspections, operators can identify and triage which components to replace first.

SLED/M can detect methane leaks as low as three (3) scfh, with a precision of 96.6% and false positive rate of 2.22%. Additionally, SLED/M is capable of estimating methane flow rate and concentration within 12% of ground truth flow rate. The technology itself only requires the MWIR OGI camera and some basic weather information; temperature, humidity, and distance from the source, providing SLED/M with a flexible competitive advantage, and reducing the need on the customer to use additional instrumentation and equipment. Figure 2 shows the progression of the algorithm through all four phases.

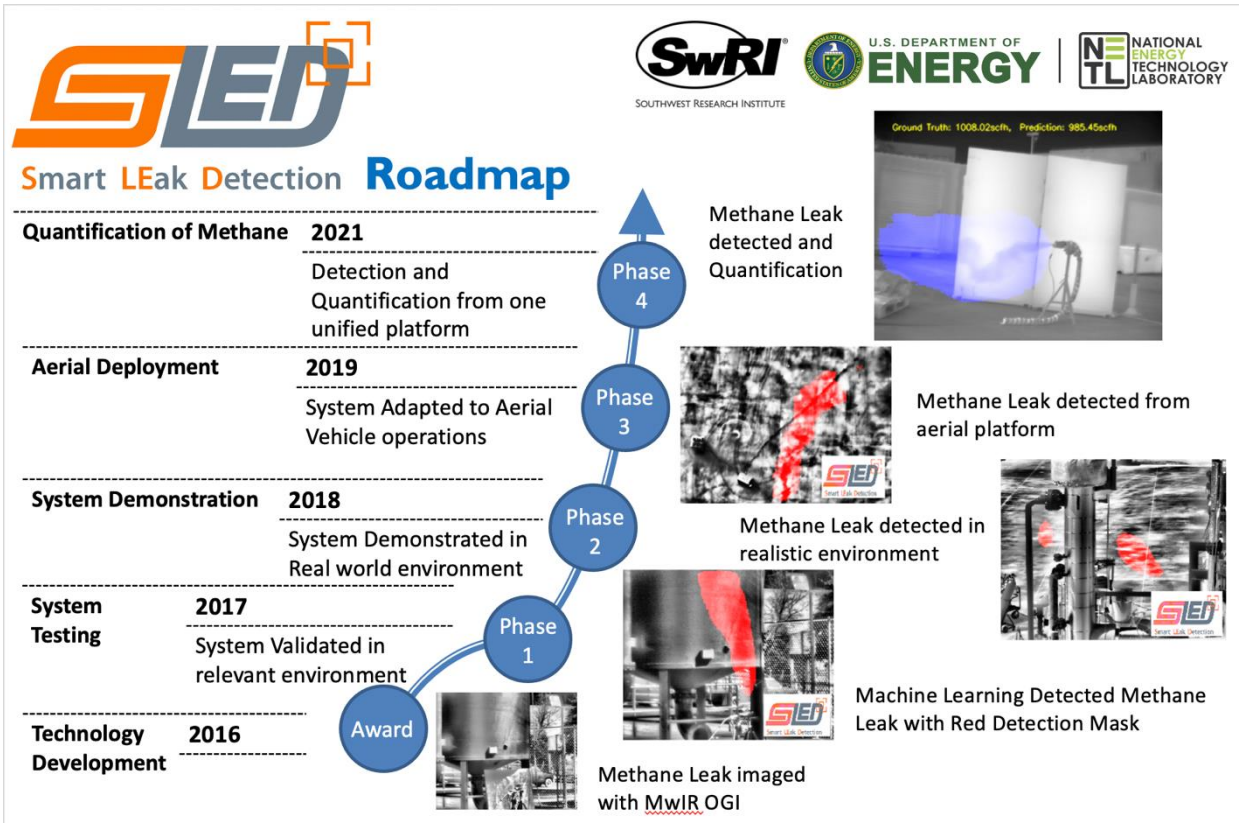

Figure 2. SLED/M Roadmap

2. PHASE 1 TECHNOLOGY DEVELOPMENT

During Phase 1, the hardware and software components of the prototype system were developed. The hardware development consisted of interfacing the electrical and mechanical components of the optical sensor with the embedded processor. The software development involved developing robust algorithms that will continuously monitor the optical sensor's output and intelligently detect the existence of methane without human intervention. The software is optimized for integration onto the embedded processor for efficient real-time execution and field operations.

2.1 Controlled Testing

SwRI continued to perform several methane release tests under realistic conditions to continue to increase the database containing methane leaks of various concentrations, distances, and scenarios. A portable rig was constructed to allow for gas discharges through various leak geometries while controlling pressure and leak rate. This was captured on the camera shown in Figure 3. The test conditions included varying ambient temperature conditions, cloud cover, presence, and lack of obstacles (such as piping), and varying wind (including stagnant) conditions.

Figure 3. Niatros™ and FLIR MWIR Cameras Acquiring Data During a Supervised Methane Release

2.2 Algorithm Development

SwRI performed further data collection to diversify the training sets for both methane imagery and false positives. It has been observed that the visibility of the methane plume, both to the human eye and to the algorithm, is highly dependent on the brightness of the object behind the methane plume since the primary detection mechanism relies on the absorption properties on the methane.

For this reason, special emphasis was placed on collecting data with backgrounds of various emissivity characteristics in the Mid-Wave Infrared (MWIR) spectrum. These included bright and dim backgrounds, vegetation, and camera shots with the plume against the sky. Figure 4 shows a few interesting cases of the plume visibility on various backgrounds.

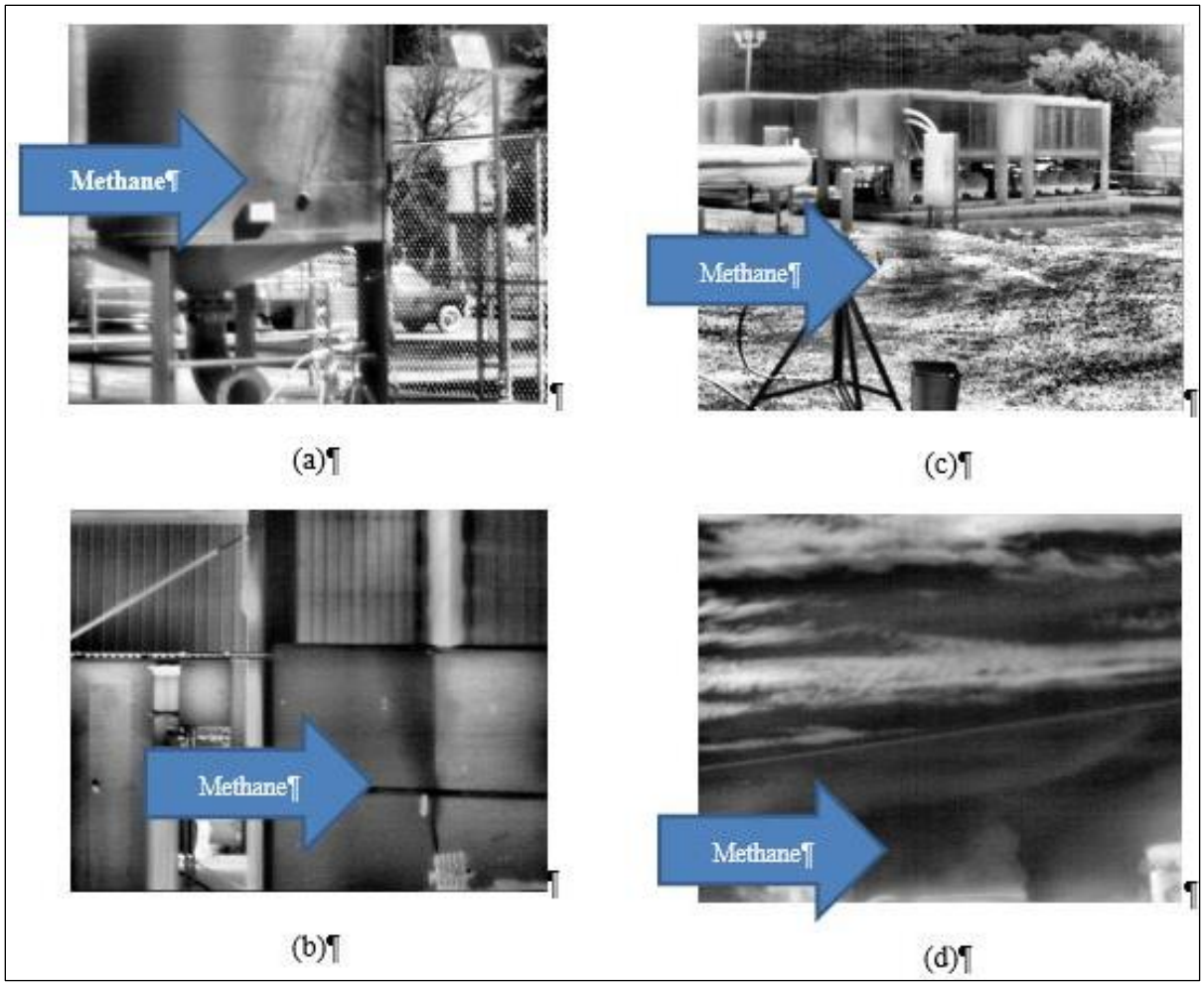

Figure 4. A Methane Plume on Background Surfaces of Various MWIR Intensities: (A) A Bright Background Object, (B) A Dark Background Object, (C) A Noisy Background Object, and (D) The Sky, Which Acts as an Infinitely Absorbing (Dark) Background and the Methane Plume

The chosen algorithmic approach uses three separate steps. First, preprocessing is used to make the methane more apparent in the MWIR imagery. The preprocessed frames are then classified using a segmentation neural network. Finally the output of the neural network is interpreted by a clustering algorithm that implements a clean tunable threshold for how sensitive the alarm reporting should be. Figure 5 shows the high-level data flow of the algorithm.

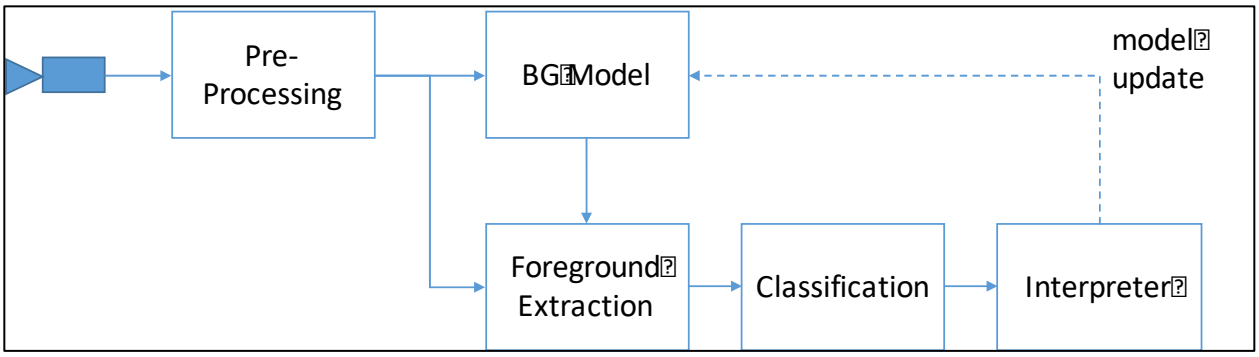

Figure 5. A Flow Chart Depicting the Data Path from Camera Acquisition to the Reporting Mechanism

Over the course of this phase, extensive work was done to identify the best-suited classifier for the detection task. The classifier must be sufficiently complex to learn the nuances of a methane plume detection while still small enough to fit within the hardware footprint of the embedded Tegra System on Chip (SoC). A variety of classifier techniques were researched and tested. Additionally, a variety of data processing and pre-processing architectures were researched. Based on this extensive effort, a processing architecture and classifier was chosen, which provided optimal results and performance. The chosen algorithm, a convolutional segmentation network, has been implemented in such a way that it will currently consume 25% of the shared memory between the Central Processing Unit (CPU) and Graphics Processing Unit (GPU).

2.3 Phase 1 Results

Error! Reference source not found. through Figure 10 highlight some of the test results from the algorithm as well as some remaining issues that needed further adjustments and training to resolve.

Figure 6. Comparison Showing Good Tracking on Steady Background

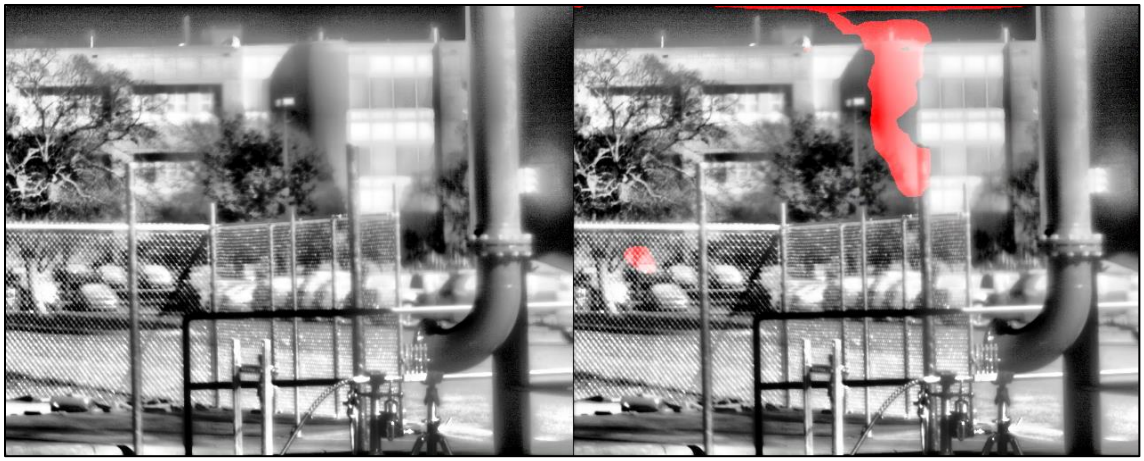

Figure 7. Comparison Showing Steady Tracking on Noisy Background, Methane Plume Not Apparent to Human Eye in Video

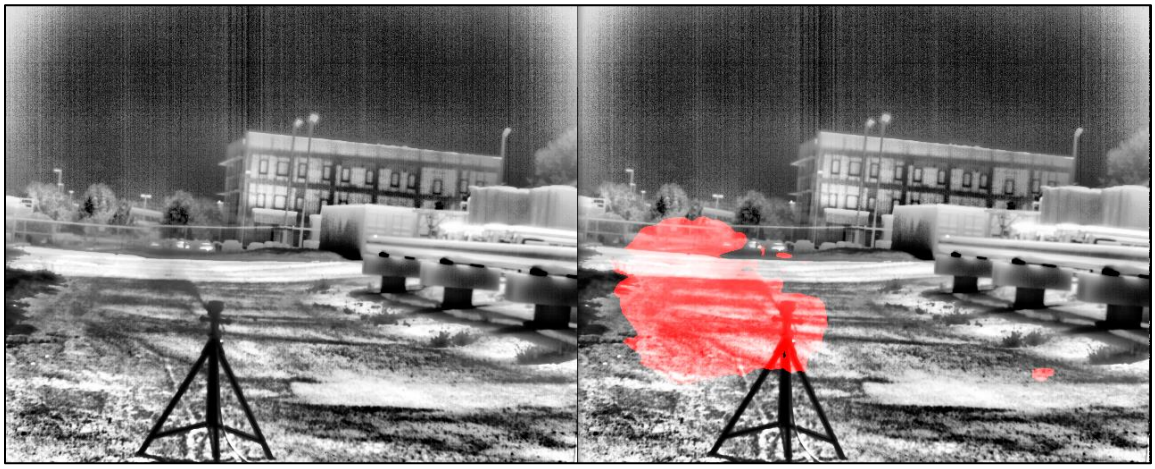

Figure 8. Comparison Showing Good Tracking on Noise Mixed Background; Persistent False Positive Present on Right Side of Image

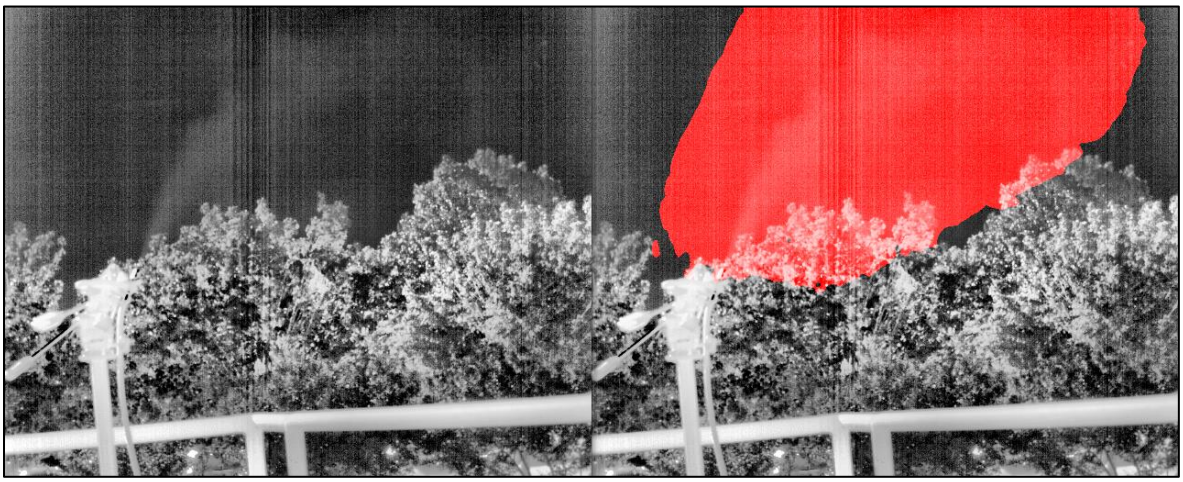

Figure 9. Comparison Showing Good Tracking of Plume in a Region of Sky, Where Optical Dynamics Vary Drastically from a Plume in Front of a Solid Reflective Background

Figure 10. Comparison Showing Good Tracking on Solid Background Again, Failures Present on Bottom-Left of Highlighted Area: Problems Persist Where High-Reflectivity Background Converges with the Plume

At the end of this phase, source code, executables, and software description documentation were delivered.

3. PHASE 2 TECHNOLOGY MATURATION

During Phase 2, the hardware and software components of the prototype system were tested and refined. The hardware testing consisted of thermal and mechanical benchmarking of the system under various connectivity and ambient temperature variations. The software testing involved collection of MWIR dataset to be used in validation of the SLED/M algorithm. This dataset was constructed to test the maximum variability in background, lighting, methane flow rate, distance to the plume, occlusions of the plume, presence of other moving and optically dynamic objects, and more. The software was optimized for integration onto the embedded processor for efficient real-time execution and field operations.

3.1 More Data Collection

The dataset utilized for testing the performance of the system and algorithm was curated through the collection of data from a variety of conditions, as well as leak and non-leak event types. This collection focused more on establishing realistic backdrops and foregrounds, as well as other sources of motion in the frames. The typical setup for data collection is illustrated in Figure 11.

Figure 11. Image of setup used for data collection at various ranges, ambient conditions, and leak types

The data was collected by saving video sequences from the camera at 5–10-minute intervals and saving these frames, uncompressed, in the .tif/.tiff format. The benchmarking dataset was extracted from this collected data by choosing sets that spanned a large range of conditions. The data was annotated by labelling which frames did and did not contain methane. The resulting benchmarking set is summarized in Table 1**Error! Reference source not found.**.

Table 1. Summary of Benchmarking Dataset

Number of Tests	183
Number of Frames	882,396
Weather	clear / rain (no methane) hot (105F) / cool (40F)
Ambient Lighting	dawn / bright / overcast / night
Wind	windy, calm
Background (in line with methane)	bright/dark/mixed
Potential False Positives	steam, CO, moving objects & people
Distances	15-700 ft
Flow rates	2 – 500 scfh

3.2 Metrics

The metrics used in this report are defined as follows:

$$True\ Positive\ (\boldsymbol{t_p}): Algorigthm\ correctly\ identified\ methane\ when\ \ present \quad (1)$$

$$True\ Negative\ (\boldsymbol{t_n}): Algorithm\ correctly\ identified\ no\ methane \quad (2)$$

$$False\ Positive\ (\boldsymbol{f_p}): Algorithm\ Identified\ methane\ when\ there\ was\ no\ methane\ present \quad (3)$$

$$False\ Negative\ (\boldsymbol{f_n}): Algorithm\ did\ not\ identify\ methane\ when\ present \quad (4)$$

$Precision = \frac{t_p}{t_p + f_p}$: Maximizing precision will minimize the false-positive errors (5)

$Recall = \frac{t_p}{t_p + f_n}$: Maximizing recall will minimize the false-negative errors (6)

$F1 = 2x\ \frac{precision * recall}{precision + recall}$: The harmonic mean of the precision and recall (7)

$$Accuracy = \frac{t_p + t_n}{t_p + t_n + f_p + f_n} \quad (8)$$

3.3 Methane Detection Benchmarks

The goals for phase 2 of development and testing, were to minimize false positives as much as possible. As such, during the system validation and testing precision, false positive rates were focused on heavily. Precision is a metric which ratios both true positives and false positives and attempts to minimize the latter. The performance of the final model is tabulated in Table 2. Figure 12 illustrates the performance of the Phase 2 algorithm on various difficult test cases.

Table 2. Performance Metrics for the SLEDM Algorithm

Metric	Score
Precision	92.9%
False Positive Rate	4.8%

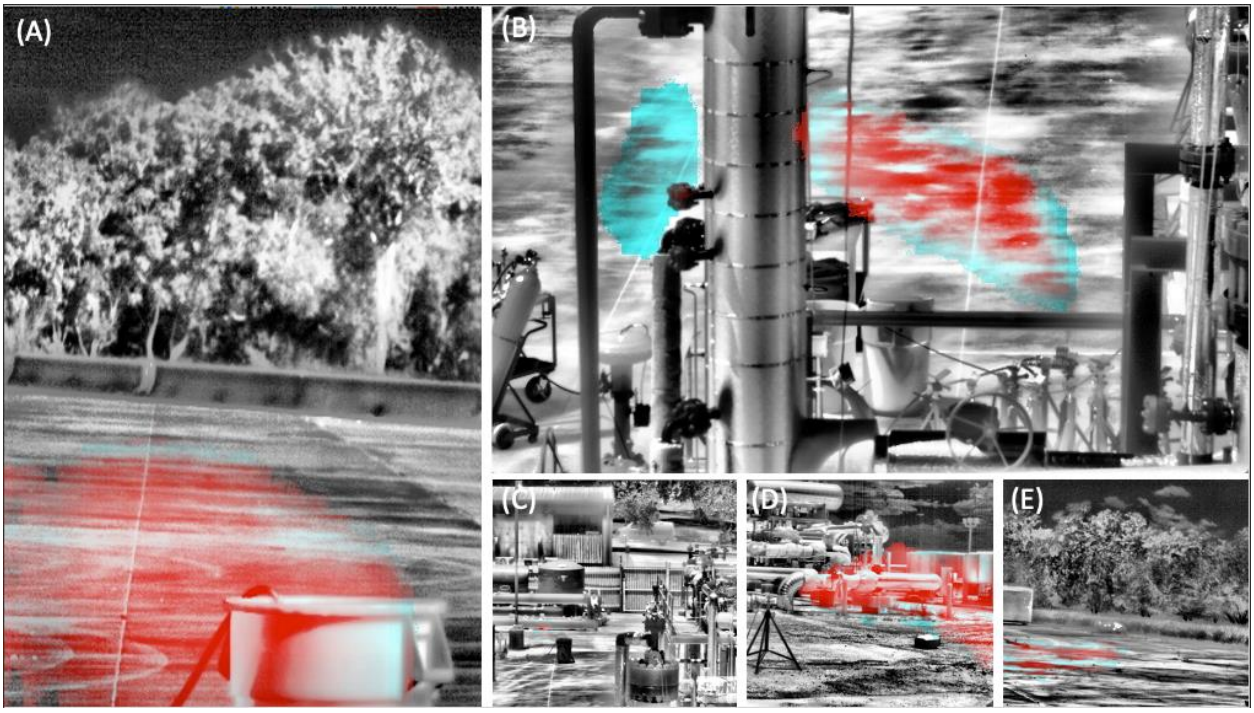

Figure 12. Figure A - Night Methane Diffused; Figure B - Foreground Occlusion; Figure C - 100m Moving Car and Vegetation (no false positives); Figure D - Highly Dynamic, Noisy Background; Figure E - Night Methane Source Out of Shot

3.4 Phase 2 Results

In Phase 2, the algorithm was retrained with even more testing from a uniquely curated dataset of methane leak imagery. Many more datasets were collected under diverse lighting, distance, and operational environments. Using this data, the algorithm was further refined, and performance tuned resulting in a system capable of automatically and reliably detecting the presence of methane gas plumes from MWIR video, while rejecting false positives such as lighting differentials, moving objects in the background, and other sources of gas clouds such as steam. We were able to get a final algorithm with 92.9% precision and a 4.8% false positive rate as show in Table 2. These metrics are a balancing act; there is room to tune the performance to favor precision and accuracy while increasing false positives, or to tune to near zero false positives while sacrificing accuracy. The resulting algorithm was able to run on an embedded Jetson TX1 SoC at 1 Hz, making it suitable for deployment.

At the end of this phase, source code, executables, and software description documentation was delivered.

4. PHASE 3 AERIAL DEVELOPMENT

The focus of Phase 3 was to update, adapt, and deploy the SLED/M algorithm on an Unmanned Aerial System (UAS). SwRI changed to a FLIR G300a OGI, which is smaller and lighter than the FLIR A6604 used in previous phases. SwRI also acquired a DJI Matrice 600 Pro UAS and DJI Ronin gimbal for data collection and testing.

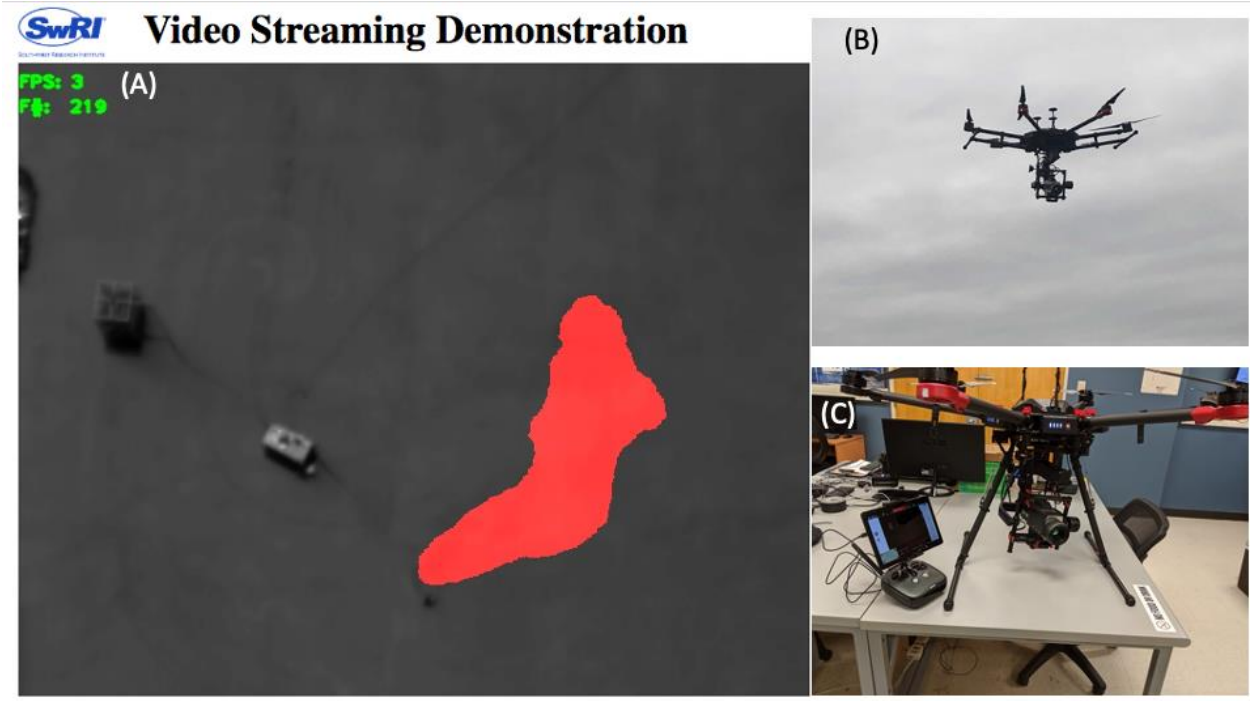

Figure 13. Figure A - SLED/M Web Based User Interface; Figure B - SLED/M System on UAS; Figure C - SLED/M Running Live Wirelessly on Drone Platform

The software was updated with a web-based user interface. This interface allows for live viewing and control of the SLED/M software and allows the system to be operated locally from a computer, tablet, or phone. Figure 13 Shows deployed SLED/M platform and wireless interfacing.

4.1 Aerial Data Collection

The dataset utilized for testing the performance of the system and algorithm was curated through the collection of data from a variety of conditions as well as leak and non-leak event types. The typical setup for data collection is illustrated in Figure 14.

Figure 14. Image of Setup Used for Data Collection at Various Ranges, Ambient Conditions, and Leak Types

The data was collected by saving video sequences from the camera at 5-10-minute intervals. Each test was taken at different angles, altitudes, speeds, and distances from the methane source. The benchmarking dataset was extracted from this collected data by choosing sets that spanned a large range of conditions. The data was annotated by labelling which frames did and did not contain methane. The resulting benchmarking set is summarized in Table 3.

Table 3. Summary of Curated Methane Dataset

Number of Tests	371
Number of Frames	1,470,039
Weather	clear / rain (no methane) hot (105F) / cool (40F)
Ambient Lighting	dawn / bright / overcast / night
Wind	windy, calm
Background (in line with methane)	bright/dark/mixed
Potential False Positives	steam, CO, moving objects & people
Distances	15-700 ft
Flow rates	2 – 500 scfh
Altitudes	50ft – 400ft

4.2 Aerial Methane Detection Benchmarks

The goals for this development cycle were to keep false positives to a minimum, while incorporating motion and altitude from the UAS, as such during system validation and testing, precision and false positive rates were focused on heavily. The performance of the final model for this phase is tabulated in Table 4. The results in Figure 15 illustrate the performance of the algorithm on various difficult test cases.

Table 4. Performance Metrics for the SLEDM Algorithm

Metric	Score
Precision	96.6%
False Positive Rate	2.22%

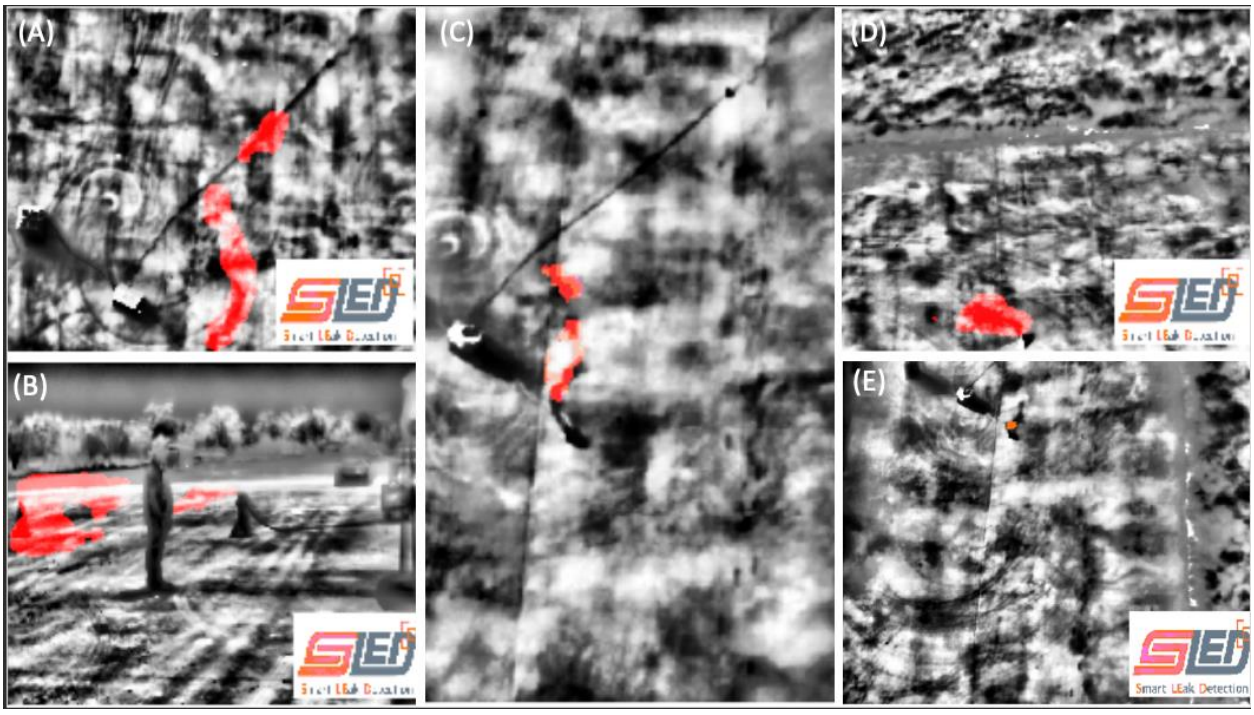

Figure 15. Figure A – Directly Above Source; Figure B – Foreground Motion Rejection; Figure C – 400 Feet Altitude; Figure D – Detection at 30 Mph; Figure E Detection from distance

4.3 Phase 3 Results

During Phase 3, the hardware and software components of the prototype system were adapted to work on an UAS. The embedded computer system was paired with an aftermarket development board for a smaller form factor; the OGI was replaced with a newer, smaller form factor and used a lighter weight camera. All of these refinements were made to the system to keep the payload as light and small as possible to optimize flight time. The SLED/M algorithm was significantly improved through tuning of the system for speed improvements, changes to the pre-processing, as well as run-time inferencing engine. Three new data sets were collected of methane releases from

both the ground and from the air at various altitudes and speed to adapt the algorithm to both the new camera system as well as train it to operate from a moving platform. SwRI integrated a FLIR G300a OGI with a DJI Matrice 600 Pro UAS and DJI Ronin gimbal. SLED/M was further trained and refined for increased reliability using a large portion of the data collected during Phase 1, Phase 2, and moving and arial data from Phase 3. The speed of the system was increased five-fold from 1.2 Hz to being capable of running at 5+ Hz. The final algorithm performance was evaluated at a 96.6% precision with a 2.22% false positive rate against all the validation data from Phase's 1, 2, and 3. The resulting algorithm can work on both stationary as well as drone-based applications.

At the end of this phase, source code, executables, and software description documentation was delivered.

5. PHASE 4 METHANE QUANTIFICATION

In Phase 4, the focus of the research was shifted from detection of methane to quantification of methane. To accomplish this, the MWIR OGI needed to be supplemented with added sensors to provide additional input for the quantification of methane. Due to the passive nature inherent in MWIR OGI technology, it has a heavy reliance on a variety of external factors, all of which have a direct impact on what is observed by the MWIR OGI. To overcome this, we started off by including several different information sources, including, but not limited to Longwave Infrared Image (LWIR), LiDAR, visible camera, and a weather station for ambient weather readings (Figure 16).

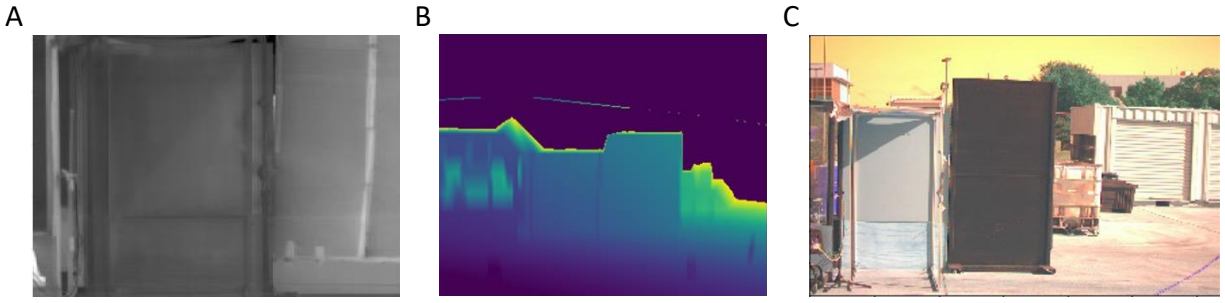

Figure 16. A) Longwave Infrared Image, B) LiDAR Distance Map, and C) Visible Image of Methane Leak

5.1 Sensor Integration, Sensor Driver Development and Stereo Camera Calibration

A LWIR thermal imager was chosen because methane has an absorbance peak in the LWIR band (Figure 16A) in addition to the MWIR band, although much smaller. While methane absorbance is not as strong in the LWIR region, these imagers are capable of methane detection by themselves. The idea behind including this image band was that LWIR could provide additional information which would inform the analysis of MWIR imagery including ambient temperature, component temperature, and the temperature delta (ΔT) of the methane plume. Specifically, integration of MWIR and LWIR data can provide important details for understanding the physics of methane, absorbance, and real-time background modeling using the aligned data from MWIR and LWIR observations.

The distance of the OGI relative to the plume and the lighting intensity are two important factors that can influence quality and accuracy of methane detection and quantification. To try to get accurate distance representation of all points within the images, a LiDAR sensor was added to the unit (Figure 16B) in an effort to get automated distance information rather than relying on the operators to input. Finally, a visible camera was added, which can give information on lighting reflections and component identification (Figure 16C).

Software was developed to integrate the sensor drivers from multiple sources in one central location. Included in the software is the capability to read and save data from the various sensors under investigation including the FLIR g300a, FLIR Boson 640, Basler acA1920, Velodyne VLP-16 Puck Lite, and ODROID WeatherBoard 2.0. Drivers were written or incorporated and optimized to run on an Nvidia Tegra TX-2 and Nvidia Xavier AGX embedded computers.

It was necessary to develop software that would generate a data fusion of the multiple disparate data sources and streams which required temporal and spatial alignment, as well as standardization. The first step in this process was to register the different camera views together, using the MWIR OGI images as the reference for alignment. Data fusion provides functionality for comparison of streams and sources relative to each other in parallel. A thermal blackbody calibration tool was used in both the MWIR and LWIR imagers for relative pixel intensity comparisons (Figure 17). Each camera has a different dynamic thermal range; the MWIR camera has a relatively small thermal window and so the pixel intensity swings from one end of the range to the other very quickly, while the LWIR camera has a much wider thermal calibration, and so stays within a much smaller window (Figure 18).

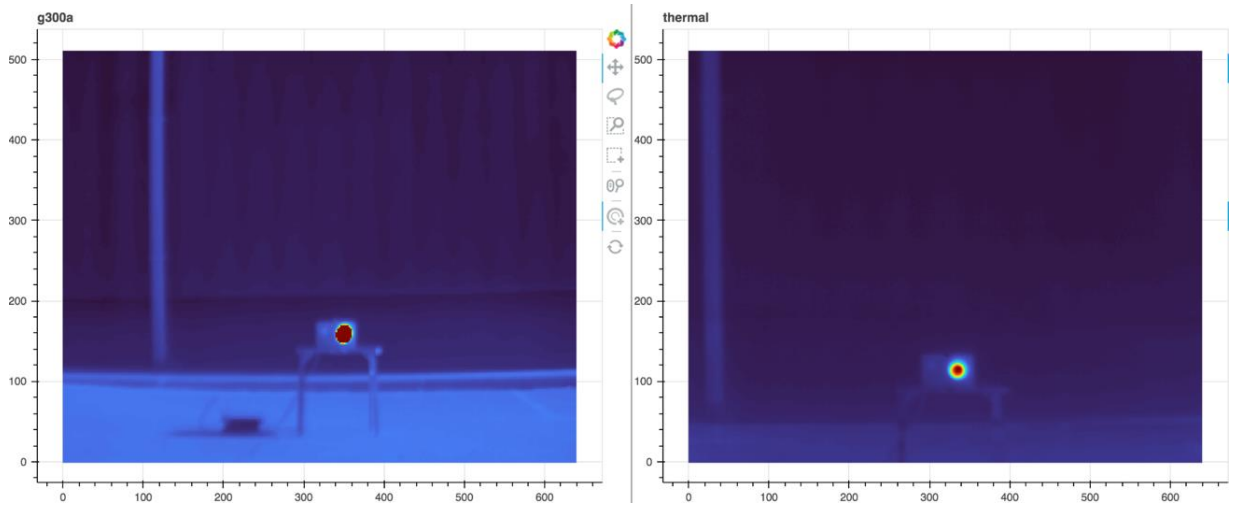

Figure 17. Thermal Blackbody Calibration Tool Observed in MWIR (Left) and LWIR (Right)

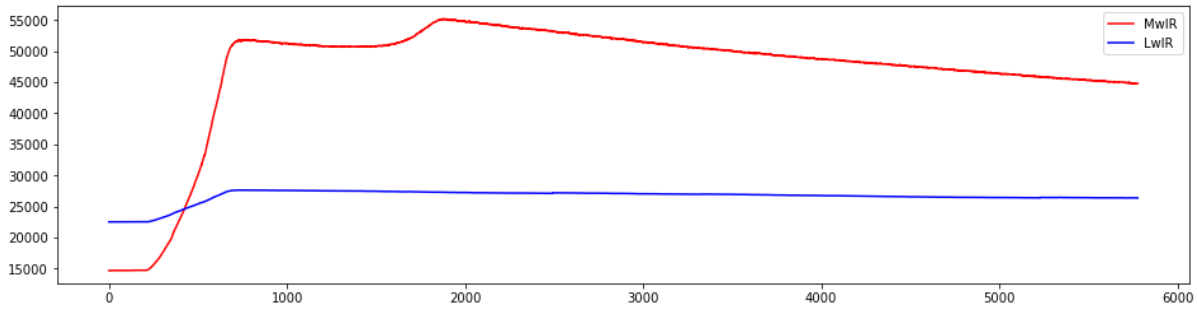

Figure 18. Pixel Intensity for Both MwIR and LwIR as Thermal Blackbody Heats and Cools

5.2 Data Collection

The initial round of data collection in September 2020 used a wind tunnel to provide additional plume stability with the configuration for the initial setup shown in Figure 19. Table 5 shows the test matrix performed during each collection.

Table 5. Summary of Methane Quantification Data Collection

Fall 2020	
Number of Test Configurations	111
Sensor Array Distance (ft)	20 – 50
Background	Solid cardboard wall, solid metal wall, no immediate backdrop
Methane Flow Rates (scfh)	0, 20 – 400
Weather	Drizzle, overcast, sunny
Wind	Calm, gusty

During the first round, the tunnel and fan setup ensured data collected during the experiment would consider “Downwind Distance” to be composed of solely one direction and relatively consistent windspeed while largely ignoring external wind. The Camera array was placed at various distances ranging from 20ft to 50ft away from the test, and the methane release flowrates varied from 0 scfh to 400 scfh. Directly behind the opening of the wind tunnel, two different solid walls were setup. One cardboard to be relatively low reflectance and thermal emission, and another metal, which has a higher visible and thermal reflectance and emissivity. Data Collection setup is shown in Figure 19. Along with the optical sensors laid out above, a portable weather station was included in the test. This station recorded UV index, Solar Radiation, Humidity, Pressure, and Temperature, all of which affect the observability and absorption of CH_4 in the MWIR band.

Figure 19. Fall 2020 Methane Quantification Setup A) Schematic B) and Actual Setup, and Sensor Setup C) Back View and D) Front View

5.3 Data Exploration

In order to understand what the methane should ideally look like in the OGI at different flow rates, we generated the ideal volumetric methane concentration of each test at the prescribed distance and release rate. We then compared the modelled concentrations with the observed methane in the corresponding test. It was noted that there is a notable correlation in regions of higher concentration in the dispersion model with areas of lower intensity (greater optical absorption) in the observed plume. The effects plume stability were also investigated, and an algorithm was developed to infer stability conditions based on observed plumes. Figure 20 shows an ideal plume model fit to the spline of an unstable detection mask. This process allows for us to account for wind and turbulence when comparing observations vs modelling.

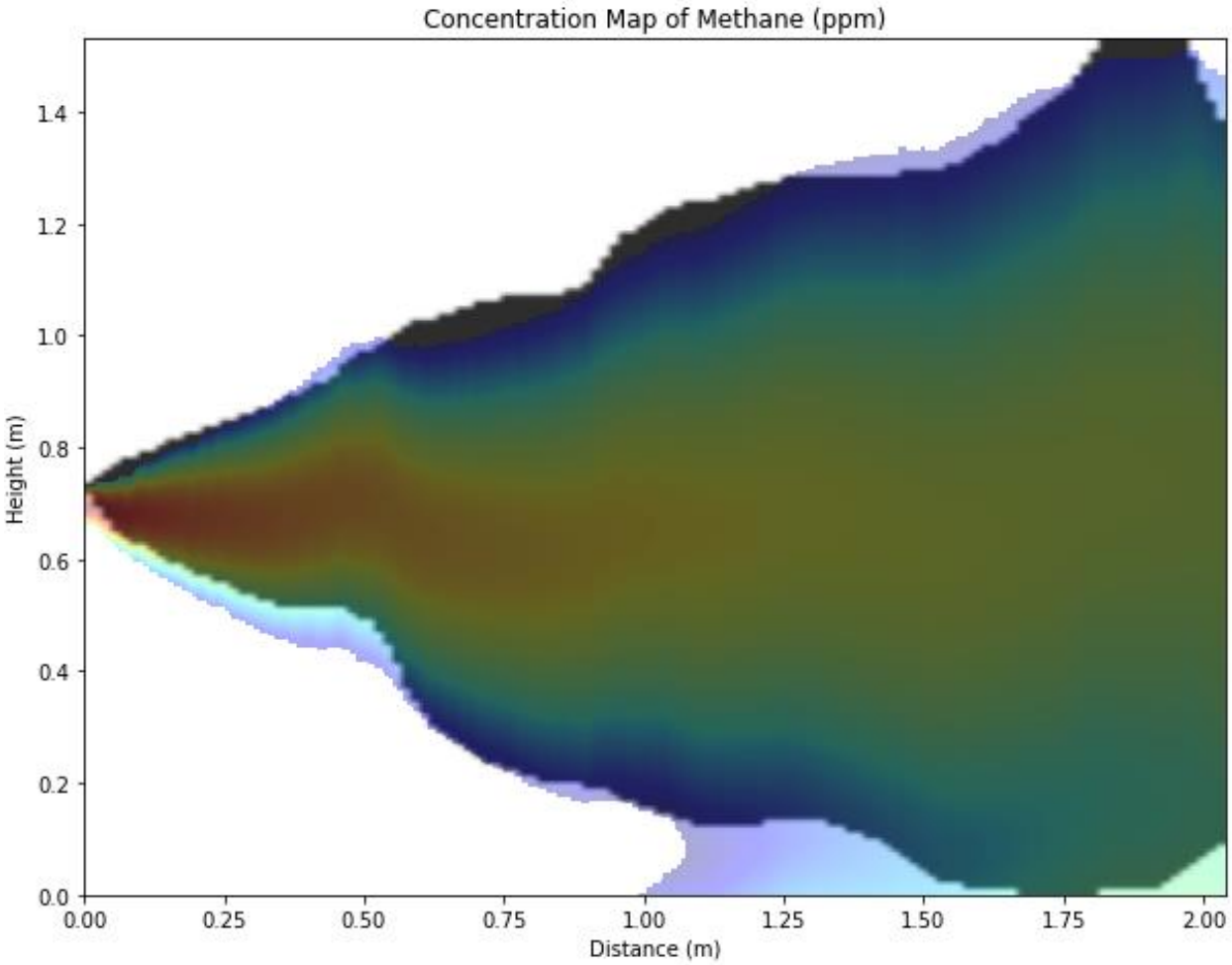

Figure 20. Gaussian Plume Model Spline Fit and Overlayed on Observed Plume

It was observed that the effect of lighting conditions on observed methane plumes plays a large role in the data as well. During data collection over the course of several days, weather ranged from completely overcast and partly raining to fully sunny on other days. These variations between each test and the UV index and Solar Radiation values changes how much radiation the methane is absorbing, and thus, how much information the OGI can obtain on the methane plume. Efforts were made to account for the observed lighting variations by incorporating information from the visible camera, LWIR camera, and weather station solar and UV sensor readings. Unfortunately, the problem is nonlinear in nature and removing the effects in the recorded MWIR band was not possible.

5.4 Go/No-Go Decision Point

The Go/No-Go Decision point for this phase of the project was defined in the U.S. Department of Energy's Statement of Project Objectives (SOPO) as:

- Develop a functioning prototype system with interfaced cameras and processing system that provides the following: Quantification of Methane plumes within +- 50% actual release for 70% of its quantification decisions.

The validation metrics for the model at the end of the first phase are shown in Table 6.

Table 6. Model Validation Metrics

Accuracy	
<=100scfh	0.84
>=150scfh	0.80
Weighted Accuracy	0.82

The first half of phase 4 was focused on identification of suitable and promising algorithms, processing techniques, and data combinations to properly inform the quantification goals. To limit the number of parameters to consider, certain constraints were imposed including the aggregation of the recorded methane flow rates into a binary thresholding problem. The tests were binarized as so:

- <=100scfh
- >=150scfh

The Go/No-Go results are based on this premise and models trained accordingly. For our validation data, we took two tests and this time we incremented the flow rate by 50 scfh every two (2) minutes in the data; one starting at 25 scfh and ending at 250 scfh, and another starting at 400 scfh and ending at 50 scfh. The metrics presented are based off of these validation tests. When classifying 25-100 scfh and 150–400 scfh as >=150 scfh, we are within the +- 50% defined goal for Phase 4a and we categorize each flowrate successfully 82% of the time, surpassing the goal of 70% accuracy in Phase 4a.

5.5 Phase 4b: Regression Model Development

The results of the September experiments were used to inform setup and data collection procedures for the second round of data collection in April 2021.

	Fall 2020	Spring 2021	Total
Number of Test Configurations	111	116	227
Sensor Array Distance (ft)	20 – 50	30	20-50, (30 spring)
Background	Solid cardboard wall, solid metal wall, no immediate backdrop	Solid metal wall	Solid cardboard wall, solid metal wall, no immediate backdrop
Methane Flow Rates (scfh)	0, 20 – 400	0, 50-1000	0 - 1000
Weather	Drizzle, overcast, sunny	Overcast, sunny	Drizzle, overcast, sunny
Wind	Calm, gusty	Calm, gusty	Calm, gusty

During the second round of data collection, the camera array was placed at a fixed distance of 30 ft. The pseudo wind tunnel and fan setup were completely removed, and a solid surface backdrop was selected to maximize the temperature differential, ΔT (Figure 21). To improve performance of training regression-based network models, the second round of testing focused more on continuous sweep tests between the range of 25 – 1000 scfh to allow for better training a validation of the system. A methane flow meter was added into the system with 10hz data logging to measure real-time flows and allow for converting from categorical networks to regression networks more accurately. The same sensors and weather station were used to observe and record the methane over a weeklong period.

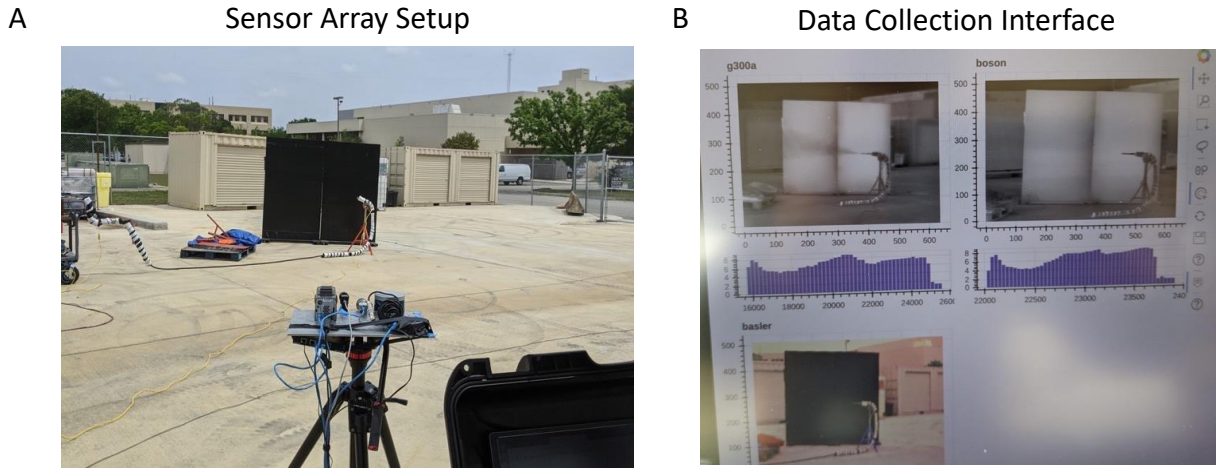

Figure 21. A) Second Round Setup and B) Collection Interface

In addition, during the second round of data collection, the effects of orifice size were investigated to see what role it may have on detection or quantification algorithm performance. In Figure 22, the blue masks represent the contour of the methane plume detected by SLED-M system. The plume becomes narrower and the distance between the upstream edge of the detected contour increases with decrease in the orifice size (d_o), while the plume becomes thicker and more easily detectable with an increase in orifice size (d_o). This lead to the observation that it is much easier to quantify the observed plumes with larger diameter orifices to reduce exit velocity of the gasses.

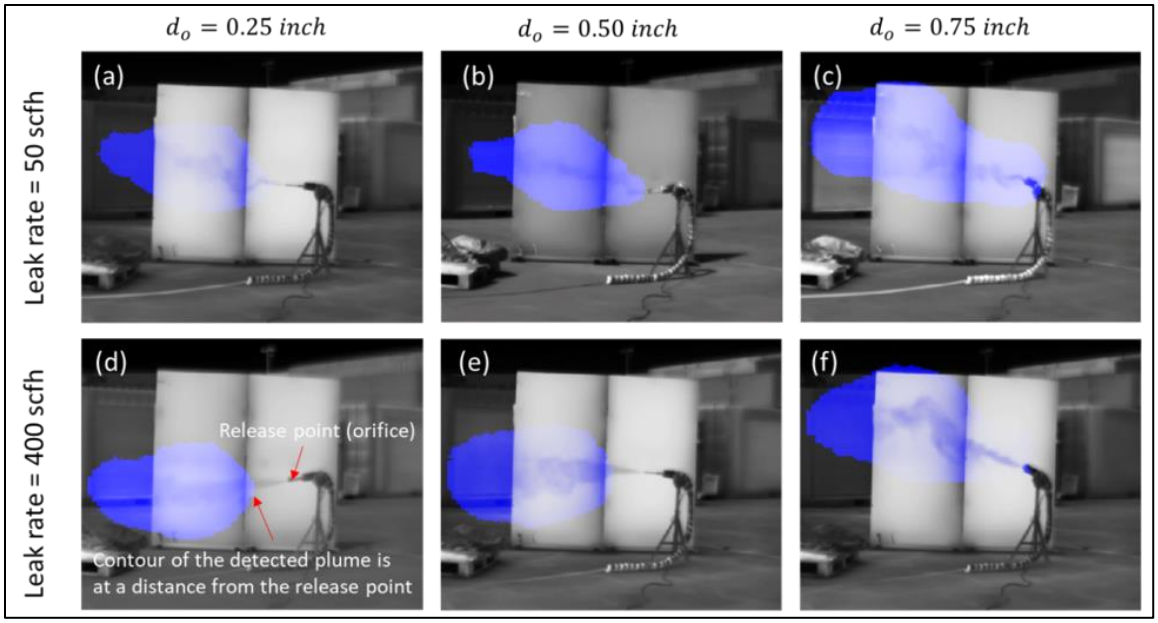

Figure 22. Effect of Orifice Size (d_o) on the Shape and Position of the Methane Plume Detected by SLED-M System for Low and High Flow Rates

5.6 Methane Quantification Performance Evaluation

During Phase 4b, SwRI explored many iterations and combinations of model training and processing. The performance of the models were evaluated against validation data and each other to monitor and track improvements in the outputs as well as hyperparameter and input relationships presented in the models. Figure 23 provides an example output of model validation after an epoch in training. The plot shows the predicted scfh value vs the ground truth scfh value at each time step and plots them as a correlation scatter plot. This allows for quickly and qualitatively evaluating the models progress and ability to learn during training. A perfect model would have one dark line going diagonally from bottom left to top right; the colors of each scatter point indicate the Mean Absolute Error (MAE) from the center of the line and thus how incorrect each guess was by the model.

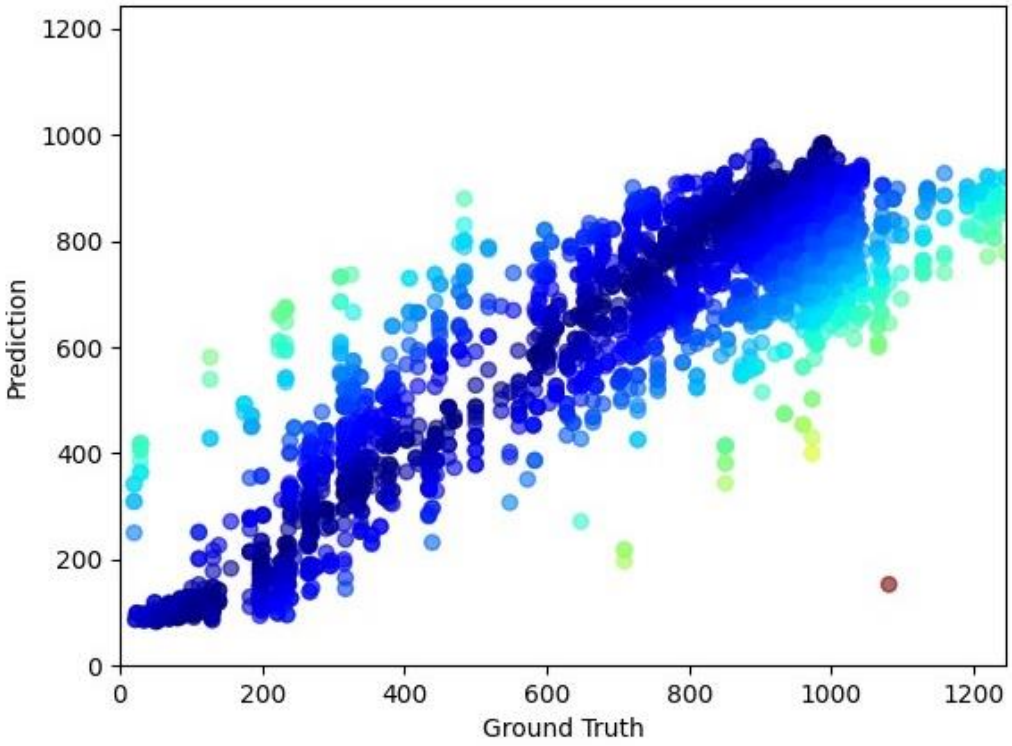

Figure 23. Example of Single Model Correlation Scatter Plot Ground Truth vs Prediction

5.6.1 Validation Data

Throughout Phase 4, the team trained and validated close to 300 models. The training and validation sets were made by splitting the collection of all sets into two groups such that the validation set had a representation across the whole tested scfh range. To increase model performance, the team applied filtering to these sets to ensure the model would make quantification attempts only if environmental conditions were sufficient to yield a good estimate. The team found that examining model performance on poor environmental conditions (e.g., very windy, great overcast, etc.) resulted in non-representative metrics, as the model expectedly struggled in these conditions. A table describing the dataset and the filtered dataset can be seen (Table 7**Error! Reference source not found.**).

Table 7. Validation Set

		group								
description	mode	50 scfh	100 scfh	150 scfh	200 scfh	250 scfh	400 scfh	1000 scfh	sweeps	totals
# of sets	train	5	3	4	5	4	4	1	9	35
	validate	1	1	1	1	0	1	0	4	9
total-count (frames)	train	20684	13826	17886	23575	17114	17396	5007	49641	165129
	validate	4297	4694	4342	4502	0	4248	0	17168	39251
filtered-count (frames)	train	9713	5673	9220	9389	9529	7937	2838	13185	67484
	validate	2603	1028	2550	2398	0	2721	0	8695	19995

The validation set was designed to provide additional detail to inform future hypotheses for model performance optimization. The set included five fixed rate and four sweep rate samples all of which spanned the range of collected flow rates between 0 and 1000 scfh. Validation set was designed to

provide additional detail to inform future hypotheses for model performance optimization. Scfh by time plots of the validation data are shown in Figure 24.

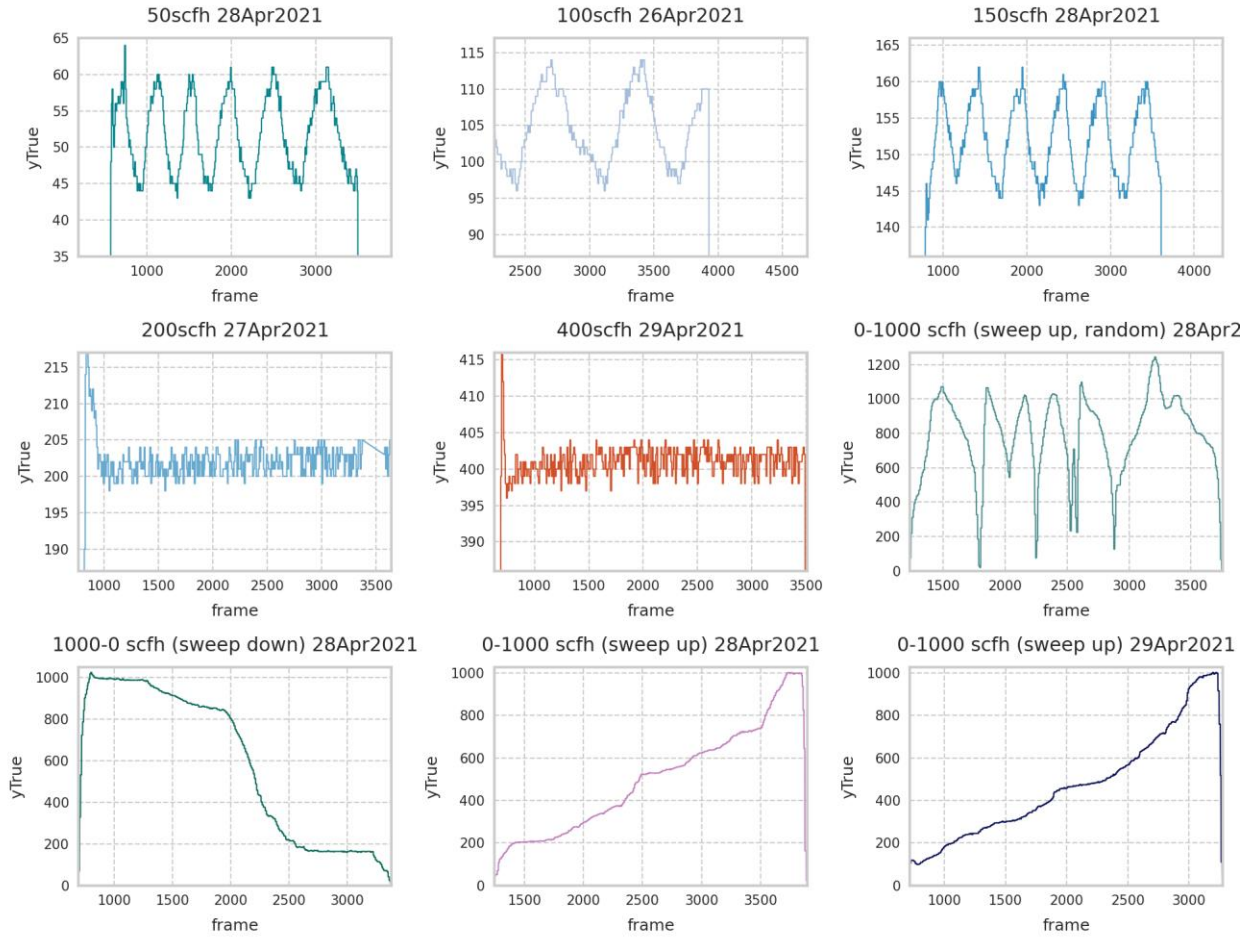

Figure 24. Validation Sets used for Model Evaluation.

It was noted that several datasets had extremely windy or overcast conditions that created non-ideal conditions for quantification and were not used for our experiments. As an example, on one collection there was light rain that halted collection for the day, extraneous weather conditions were outside of scope and required to be removed from the final used data. On this note, the team saw a significant difference in the fall collection and the spring collection in both the midwave and thermal sensor readings. The fall collection has much less pronounced methane sensing and had worse weather conditions overall. In addition, collection in the fall included moving in and out different backgrounds which resulted in increasing the number of experimental parameters outside of the scope of what was to be expected from our initial models. For these reasons, the team primarily used the April collection and split that collection into training and validation sets.

5.6.2 Sensor Combination Evaluations

To evaluate the efficacy of the midwave, longwave, and visible sensors used in data collection, an experiment involving camera combinations at varying flow rates was performed. The initial hypothesis was that additional sensors provided as inputs to supplement the midwave sensor would improve lead to improvements in regression model performance. Five combinations of sensors

were evaluated, and feature engineering was used to add additional temperature information for some combinations. Three pre-trained deep learning models with pre-trained weights were used, including InceptionResNetV2, MobileNetV2, and EfficientNetB0. These five combinations of sensors were trained and tested against the validation data.

To validate and compare each model, prediction values per frame were generated. A rolling median was calculated for smoothing the predicted results using a window size of 50 frames. Frames in which a true value flow rate of less than 25 or greater than 1100 scfh were removed. Calculations were performed to compute standard regression metrics including MAE and coefficient of determination (R^2) to measure performance of predictions against ground truth values. Specific to the goals of this project, mean absolute percentage error (MAPE) was also included to give a better assessment of how the model performs at lower flow rates. MAE calculations were used to rank the 15 models, which were then compared with MAPE and R^2 values for additional context. The results of this cross validation are shown in Figure 25 and Figure 26. It was noted that in general the midwave infrared + weather information performed better than combinations with thermal or visible camera pairs.

	model_cameraCombination	MAE mean	MAE median	R2 mean	R2 median	MAPE mean	MAPE median
1	EfficientNetB0 mwT	131.221	99.338	-56.583	-7.590	0.490	0.413
2	EfficientNetB0 mwT + vis	132.315	129.759	-24.867	-1.113	0.360	0.391
3	EfficientNetB0 mwT + lwT	145.790	137.713	-130.071	-44.692	0.717	0.425
4	EfficientNetB0 mw	148.956	109.835	-61.562	-7.154	0.516	0.445
5	EfficientNetB0 mwT +lwT +vis	170.256	152.098	-148.300	-19.434	0.768	0.486
1	InceptionResNetV2 mwT	107.761	92.144	-42.605	-20.207	0.470	0.342
2	InceptionResNetV2 mwT + vis	113.927	126.763	-63.446	-41.853	0.545	0.397
3	InceptionResNetV2 mwT + lwT	120.811	81.202	-22.375	-5.054	0.379	0.401
4	InceptionResNetV2 mw	121.055	75.764	-37.040	-17.097	0.449	0.414
5	InceptionResNetV2 mwT + lwT + vis	126.703	87.989	-24.196	-19.571	0.375	0.387
1	MobileNetV2 mwT + vis	109.661	113.948	-22.710	-6.874	0.340	0.349
2	MobileNetV2 mwT	112.152	109.777	-31.321	-29.154	0.432	0.358
3	MobileNetV2 mw	114.712	109.373	-31.827	-17.028	0.425	0.348
4	MobileNetV2 mwT + lwT + vis	115.325	93.195	-72.017	-14.912	0.568	0.400
5	MobileNetV2 mwT + lwT	117.469	89.498	-58.211	-5.634	0.515	0.392

Figure 25. Camera Combination Evaluation Results.

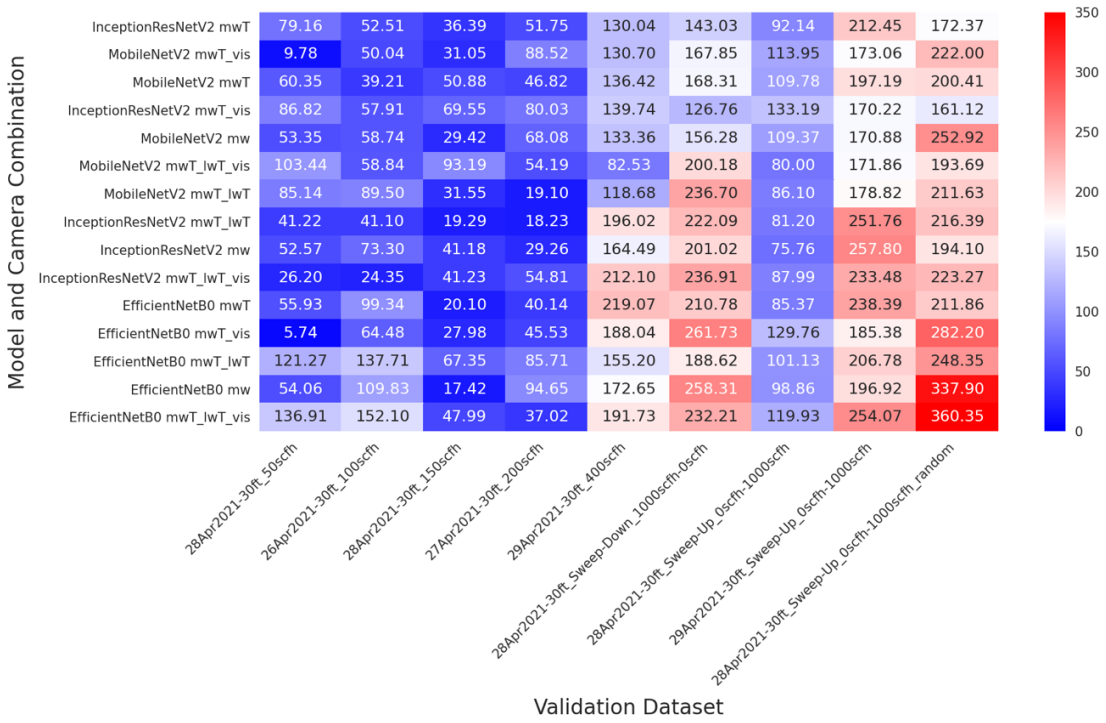

Figure 26. Mean Absolute Error (MAE) calculations for camera combination.

5.7 Quantification Model selection

The first wave of sets was trained and validated on the set described in Table 7. The results of this set can be seen in Figure 27. The team notes that models, overall, preformed the best in the 200 scfh example and the worst in the 50 scfh example. A closer examination of the 50 scfh displayed less than optimal environmental conditions, despite attempts to filter out all these conditions, and the team notes that further exploration of filtering techniques can lead to better quantification guesses. Most models perform within 10%-30% MAPE. The team utilizes MAPE as the primary metric, as saturation in sensor data was observed for higher flowrates and less accuracy in higher flowrates is expected. The use of MAPE also artificially inflates the lower, 50 scfh flowrates by expecting a much smaller window of tolerance than the higher flowrates.

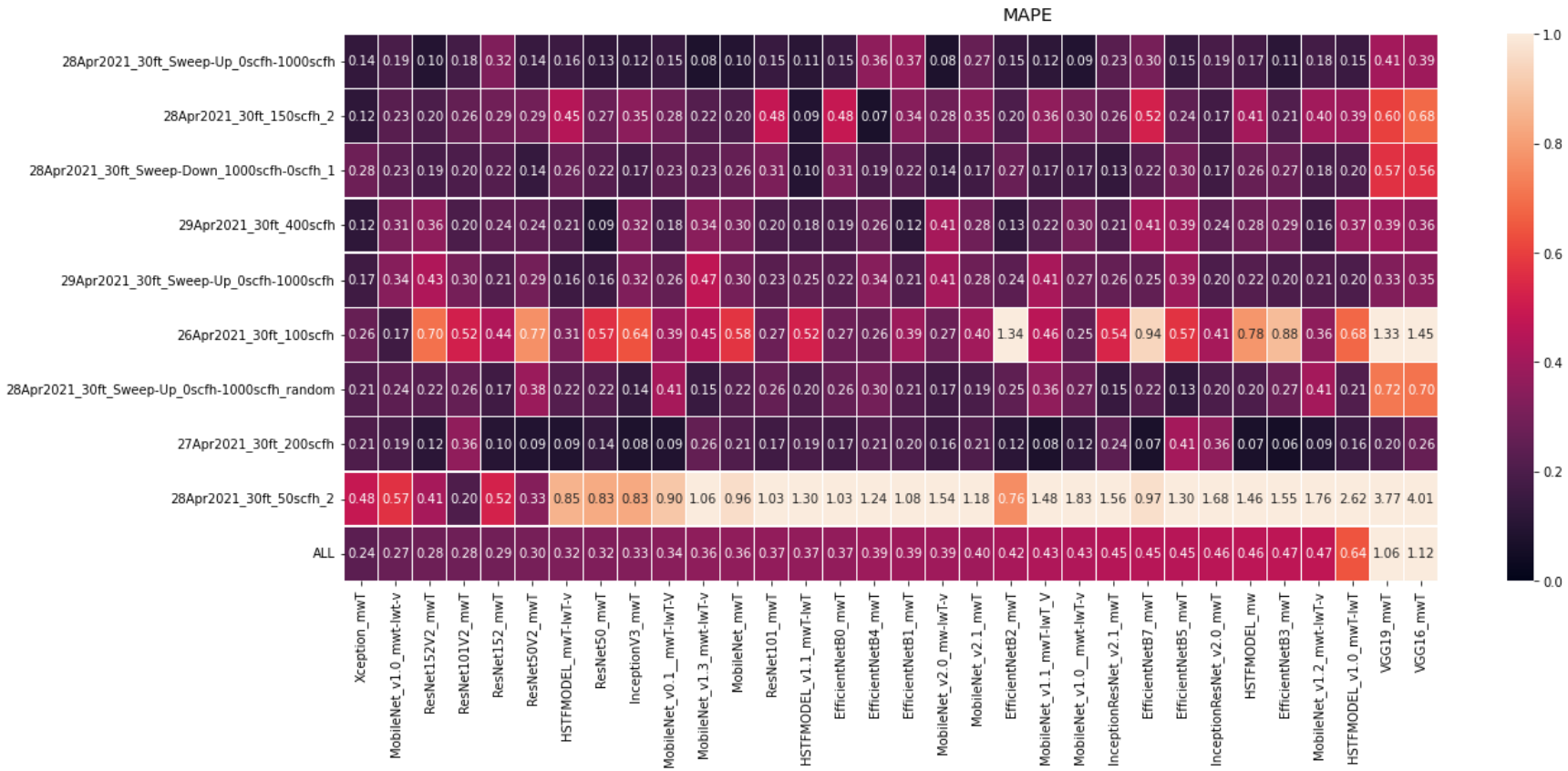

Figure 27. Mean Absolute Percentage Error (MAPE) for all sets.

Final metrics selections were made using cross-validation. Each model was passed through four (4) sets of different train/test split. Each split was set to randomly include members of static sets and sweep sets. The results of this cross validation are shown in Figure 28 with the top three regression models shown. EnsembleNet was chosen as it is the highest performer, on average, across all cross-validation sets. In addition, EnsembleNet also made use of the single MW camera which is advantageous for fielding. While the MobileNet model preformed similarly (and better in V2), the cost of using all cameras introduces significant computation complexity with non-significant improvements.

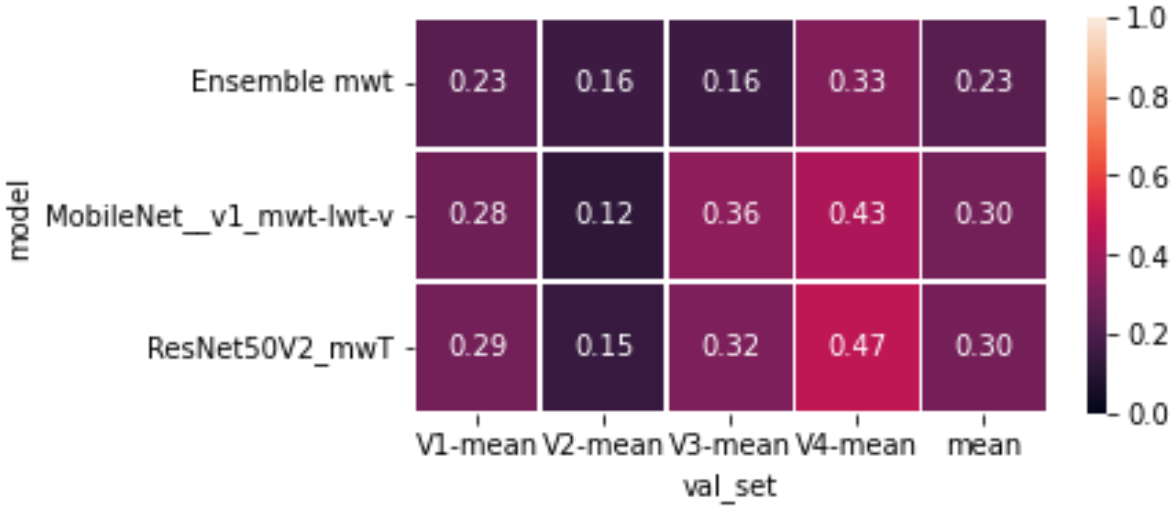

Figure 28. Model Cross-Validation Summary

5.8 Quantification Results

As mentioned, an important aspect of being able to visualize and quantify the methane, is having a valid temperature difference (ΔT) between the methane and its backdrop. When developing these metrics, they are focused on segments of methane releases that meet the following criteria:

1. SLED/M Detection is able to detect and mask the methane plume in the image and subsequent images in time
2. An adequate ΔT, ≥ 2°C, has been calculated and is present in the image

The target performance goals for this project were as follows:

1. Classification: Achieve ±50scfh Quantized Accuracy > 70% of the time
2. Regression: Achieve ≤ 10 scfh prediction > 70% of the time

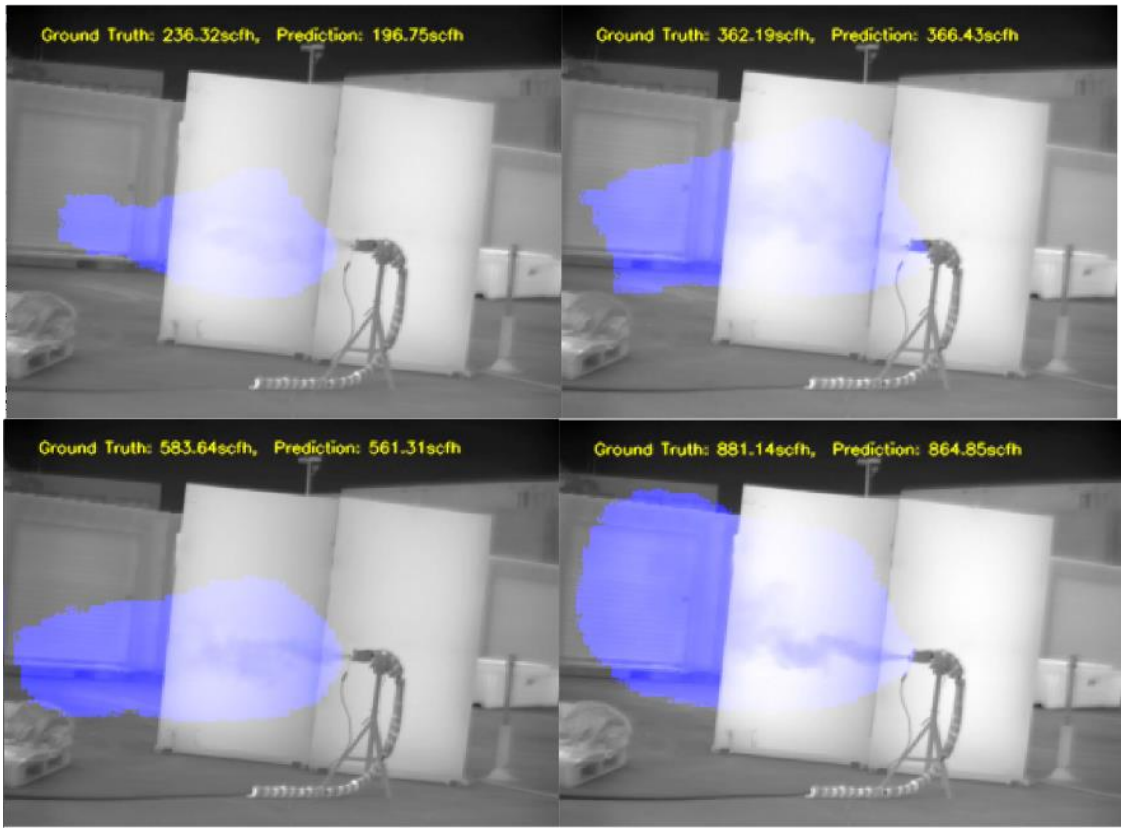

Figure 29. Detection + Quantification at Multiple Flowrates

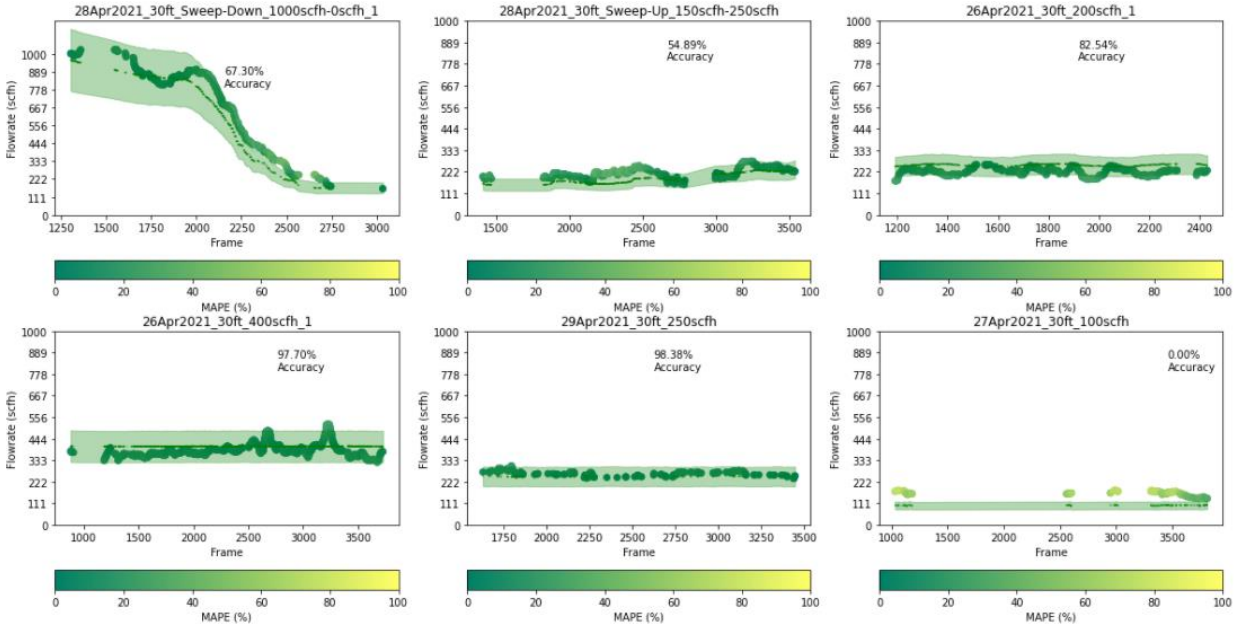

Figure 30. Final Validation Metrics

Figure 29 shows the ground truth vs predicted error for the final test data set. In addition to the MAPE, each plot has an error envelope (light green); this envelope is ± 50 scfh of the measured ground truth when below 500 scfh and ± 10% of the measured ground truth when above 500 scfh;

allowing us to bin the predictions into an accuracy score in addition to the regression error. Furthermore, we included data from various days to test the capabilities of the system in various lighting and weather conditions. Notably, the test from the bottom right most plot from the 27 of April has a lot of frames that did not meet the stability and ΔT requirements, and as such does not start stabilizing toward the end of the test, causing outliers in the statistics. This does show that the cameras are extremely sensitive to ambient conditions when making determinations, and further work is needed to combat this.

Our best performing quantification model was able to achieve the following metrics on valid frames where 1) the methane was detected and 2) a valid ΔT was observed. These results are shown in Figure 29 and **Error! Reference source not found.**.

1. Average Percentage Prediction Error: 12.3%
2. Accuracy ±50scfh: 97.78%

5.9 System Benchmarking

A key component of this last phase of the project was the commercialization and business development plan. To this end, development and benchmarking of the algorithm on embedded architectures was performed. The FLIR G300a operates nominally at 12hz and the Sierra Olympics Ventus OGI operates nominally at 30hz. Table 8**Error! Reference source not found.** shows the performance of SLED-M and SLED-Q on different embedded architectures. The Input Size fields represent the input image size in pixels to the algorithms being tested. The FLIR G300a has an output resolution of 240x320 and the Sierra Olympics Ventus OGI has an output resolution of 512x640. While operating on the highest resolution images possible is ideal, in the final application these images can be scaled for performance with minimal decrease in accuracy of the algorithms. The networks benchmarked below was trained using FP32 precision and then the trained network weights were quantized during inference for each step below.

These benchmarks can be used to inform vendors on what processing architectures to incorporate either into the cameras or into third party addons for the cameras in order to deploy SLED-M. Other Edge AI capable devices exist on the market, such as Google Coral and Intel Neural Compute Models. The boards below are what we had on hand during development.

Table 8. System Performance Benchmarks

	Model	Precision	Input Size	Frames Per Second
Xavier AGX	Detection	FP16	240x320x5	48.66 FPS
	Detection + Quantification	FP16	240x320x5, 240x320x1	30.82 FPS

6. CONCLUSIONS

Oil and gas operators need a way to reliably detect and quantify fugitive methane emissions in order to promptly act on leaks, reduce cost and risk, speed up inspection times, monitor remote and harsh environments, and satisfy recent methane regulation requirements. SLED/M helps operators to meet these needs using an autonomous, flexible technology that prioritizes safety, ease of use, reliability, and cost reduction.

SLED/M has the ability to autonomously detect fugitive methane emissions deployable on a drone for remote inspection and faster, more reliable site inspections, as well as the ability to quantify detected plumes in one tool while keeping operators out of hazardous areas. This technology can meet some customer needs including an increase in speed of periodic pipeline inspection by augmenting visual inspection for the operator, allowing them to focus on safety and other cost and risk reductions.

SLED/M can detect methane leaks as low as three (3) scfh with a precision of 96.6% and false positive rate of 2.22%. Additionally, SLED/M is capable of estimating methane flow rate and concentration within 12.3% of ground truth flow rate. The technology itself only requires the MWIR OGI camera providing SLED/M with a flexible competitive advantage and reducing the need on the customer to use additional instrumentation and equipment.

6.1 Next Steps

During development of the quantification algorithm, it was noted that environmental factors play a large role in the reliability of the outputs. Further data collections and work is needed to develop a robust quantification dataset, varying environmental lighting, weather, distance, and backdrops. Additionally, reliably recording and correlating all of this information has been a problem, so further work is needed on developing robust testing setup and methodologies for future work.

7. ACKNOWLEDGEMENT

The project team gratefully acknowledge that this work is supported by the U.S. Department of Energy's Office of Fossil Energy and the National Energy Technology Laboratory (NETL) , under Award Number DE-FE0029020. The team also gratefully recognizes significant support and collaboration from Teledyne-FLIR, Sierra Olympics, and Heath Consultants.

8. DISCLAIMER

9. REFERENCES

[1] D. J. Zimmerle *et al.*, "Methane Emissions from the Natural Gas Transmission and Storage System in the United States," *Environ Sci Technol,* vol. 49, no. 15, pp. 9374-83, Aug 4 2015, doi: 10.1021/acs.est.5b01669.

[2] R. Subramanian *et al.*, "Methane emissions from natural gas compressor stations in the transmission and storage sector: measurements and comparisons with the EPA

greenhouse gas reporting program protocol," *Environ Sci Technol,* vol. 49, no. 5, pp. 3252-61, Mar 3 2015, doi: 10.1021/es5060258.

[3] D. R. Johnson, A. N. Covington, and N. N. Clark, "Methane Emissions from Leak and Loss Audits of Natural Gas Compressor Stations and Storage Facilities," *Environ Sci Technol,* vol. 49, no. 13, pp. 8132-8, Jul 7 2015, doi: 10.1021/es506163m.

[4] A. P. Ravikumar *et al.,* "Single-blind inter-comparison of methane detection technologies – results from the Stanford/EDF Mobile Monitoring Challenge," *Elementa: Science of the Anthropocene,* vol. 7, 2019, doi: 10.1525/elementa.373.

DELIVERABLES REPORT

PHASE 4 DELIVERABLES REPORT

for the

SMART METHANE EMISSION DETECTION SYSTEM DEVELOPMENT

10.22468-DELIV_REPORT-01
Rev 0 Chg 0
November 2021

SwRI® Project No. 10.22468

PREPARED FOR:

U. S. Department of Energy
National Energy Technology Laboratory
WORK PERFORMED UNDER AGREEMENT: DE-FE0029020

SUBMITTED BY:

Heath Spidle, Principal Investigator
heath.spidle@swri.org
(210) 522-6717

SOUTHWEST RESEARCH INSTITUTE®
6220 Culebra Road, San Antonio, Texas 78228-0510
(210) 684-5111 • FAX (210) 522-5499

PHASE 4 DELIVERABLES REPORT

for the

SMART METHANE EMISSION DETECTION SYSTEM DEVELOPMENT

10.22468-DELIV_REPORT-01
Rev 0 Chg 0
November 2021

SwRI® Project No. 10.22468

Prepared by: _____ Date: 11/18/2021
Heath Spidle, PI – Southwest Research Institute

Approved by: _____ Date: 11/18/2021
Marisa Ramon, Manager R&D – Southwest Research Institute

REVISION NOTICE

Version Identifier	Date of Issue	Summary of Changes
Rev 0 Chg 0	December 2021	Initial issue

This document contains information that is as complete as possible. Where final numerical values or specification references are not available, best estimates are given and noted To Be Reviewed (TBR). Items which are not yet defined are noted To Be Determined (TBD). The following table summarizes the TBD/TBR items in this revision of the document, and supplements the revision notice above.

Section	Description

TABLE OF CONTENTS

LIST OF FIGURES

LIST OF TABLES

1. SCOPE

The major goal of this Department of Energy (DOE) research project was to develop an autonomous, real-time methane leak detection technology, The Smart Leak Detection – Methane (SLED/M), which applies machine learning techniques to passive optical sensing modalities to mitigate emissions through early detection, as well as provide a quantification estimation.

1. Run in real-time on the edge (>= 12 Hz)
2. Classification: Achieve less than 5% false positive detection
3. Classification: Achieve >= 95% methane plume detection rate
4. Regression: Achieve +- 10 scfh prediction > 70% of the time

This document summarizes the system products resulting from the culmination of the DOE-NETL Smart Methane Emission Detection System Development project.

1.1 System Overview

The Smart Leak Detection – Methane + Quantification system was developed and tested on the Nvidia Tegra Xavier AGX platform using a FLIR g300a Optical Gas Imager (OGI), with the addition of an ODROID Weatherboard 2 for real-time ambient weather conditions. The software reads frames from the OGI camera over a Real Time Streaming Protocol (RTSP) interface, and weather information over an I2C interface. This information is pre-processed and the OGI frames are fed to a pre-trained TensorRT semantic segmentation inference engine to detect and localize methane in the frame. If methane is detected, the associated OGI image and weather information is then fed to another set of preprocessors and fed to a second pre-trained TensorRT deep regression network inference engine to estimate the flow rate in standard cubic feet per hour (scfh) of the detected methane plume. Both outputs of the inference engines are then passed through post-processing functions and then displayed to the user over a web interface or RTSP output stream.

This software is capable of running >= 40 frames per second on the NVIDIA Tegra Xavier AGX platform, where the associated OGI camera is only capable of capturing images at 12 frames per second, exceeding real time capabilities of the system.

This document contains an overview of the Phase four (4) software, a description of the development and testing platform, compilation and execution instructions, and version information.

1.2 Referenced Documents

The following documents, of the exact issue shown, were referenced as indicated during the development of this document. The applicability statement associated with each document reference indicates *Superseding* if the referenced document supersedes this document in the event of a conflict.

Document ID: SwRI Proposal in Response to DE-FOA-0001538, Area of Interest 1-C
Originator: Southwest Research Institute, San Antonio, TX
Issue: June 13, 2016
Title: Project Narrative for Development of Methane Leak Detection Technology for Compressor Stations
Applicability: Defines the need for this deliverable

1.3 Acronyms

ACRONYM	DEFINITION
API	Application Programming Interface
BG	Background
CPU	Central Processor Unit
CSC	Computer Software Components
DOE	Department of Energy
GUI	Graphical User Interface
HTTP	Hypertext Transfer Protocol
I/O	Input/Output
IP	Internet Protocol
MWIR	Mid Wave Infrared
OS	Operating System
RTSP	Real Time Streaming Protocol
SD	Secure Digital
SLED/M	Smart Leak Detection - Methane
SLED/MQ	Smart Leak Detection – Methane + Quantification
SLED/Q	Smart Leak Detection - Quantification
SSH	Secure Shell
SW	Software
SwRI	Southwest Research Institute
TBD	To Be Determined
TBR	To Be Reviewed
UI	User Interface

ACRONYM	DEFINITION
UAS	Unmanned Aerial System

2. SOFTWARE OVERVIEW

The software and embedded system is collectively referred to as "SLED/M", which is a machine learning algorithm within an embedded software package. This section describes the following for the SLED/M software:

1. High-Level Software Design
2. Development and Testing Platform
3. High-Level Source Tree Description
4. Compilation and Execution Instructions
5. Version Information

2.1 High-Level Software Design

The Smart Leak Detection – Quantification (SLED/Q) software is comprised of the following components:

- Neural Network: The output of training a deep learning algorithm against a variety of methane leaks and ambient backgrounds. The neural nets produced from the training are used as inputs to the SLED/M program.
- Camera Driver: Logic that interfaces to the primary sensor, the FLIR G300a Mid Wave Infrared (MWIR) camera. In addition, the camera driver includes camera simulation logic, allowing previously recorded images to be replayed for testing purposes.
- Preprocessing: Logic that modifies the input image from the camera in preparation for the neural net and user output display. This logic is also responsible for keeping global and batch-level statistics that are used to normalize the imagery data at various stages.
- Post Processing: Logic that processes the output of the neural network and generates the user output indicating presence (or non-presence) of a methane leak.

Figure 1 depicts the logical flow of each component.

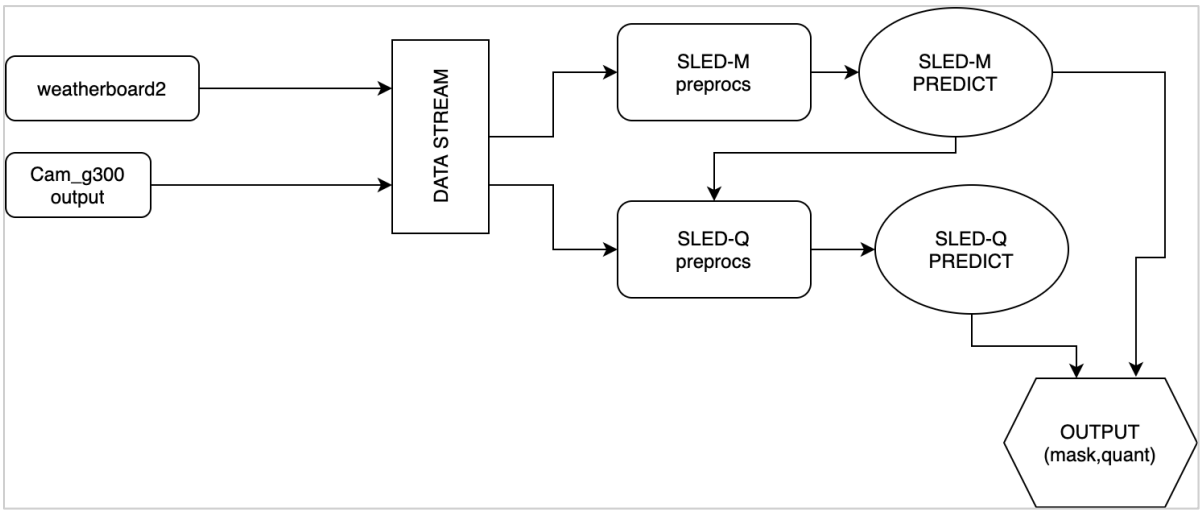

Figure 1. SLED/Q Software Flow Diagram

2.2 Development and Testing Platform

The SLED/Q software was developed on Ubuntu 18.04 LTS and tested on the Nvidia Tegra TX-2 Ubuntu 18.04 LTS, as well as the Nvidia Xavier AGX Ubuntu 18.04 LTS. System dependencies and versions are shown in Table 1; Python package dependencies and versions are shown in Table 2.

Table 1. SLED/Q System Dependencies

Package Name	Package Version
L4T	32.4.4
Jetzpack	4.4.1
Python	3.6.9
Cuda	10.2.89
TensorRT	7.1.3.0
nvinfer	7.1.3.0
cudnn	8.0.0.180
cublas	10.2.2.89-1
cudart	10.2.2.89-1
uff-converter	7.1.3-1+cuda10.2
opencv	4.1.1
protobuf	3.0.0-9.1
gstreamer	1.14.5
libboost-all-dev	1.65.1.0ubuntu1

Table 2. SLED/Q Python3 Package Dependencies

Python Package Name	Python Package Version
argparse	1.1
re	2.2.1
tensorrt	7.1.3.0
ctypes	1.1.0

Python Package Name	Python Package Version
numpy	1.18.5
numpy.core	1.18.5
numpy.core._multiarray_umath	3.1
platform	1.0.8
numpy.lib	1.18.5
numpy.linalg._umath_linalg	b'0.1.5'
zlib	1
decimal	1.7
logging	0.5.1.2
cv2	4.1.1
pycuda	(2020, 1)
six	1.15.0
decorator	4.1.2
numba	0.53.1
yaml	5.3.1
llvmlite	0.36.0
optparse	1.5.3
json	2.0.9
numba.misc.appdirs	1.4.1
scipy	1.5.4
scipy._lib._uarray	0.5.1+49.g4c3f1d7.scipy
fast_histogram	0.9
gi	3.26.1

2.3 High-Level Source Tree Description

The components previously described in Section 2.2 are split among several subdirectories in the SLED/M source tree, Table 3 provides a listing of the primary source files and directories. Figure 2 shows the data flow of the program.

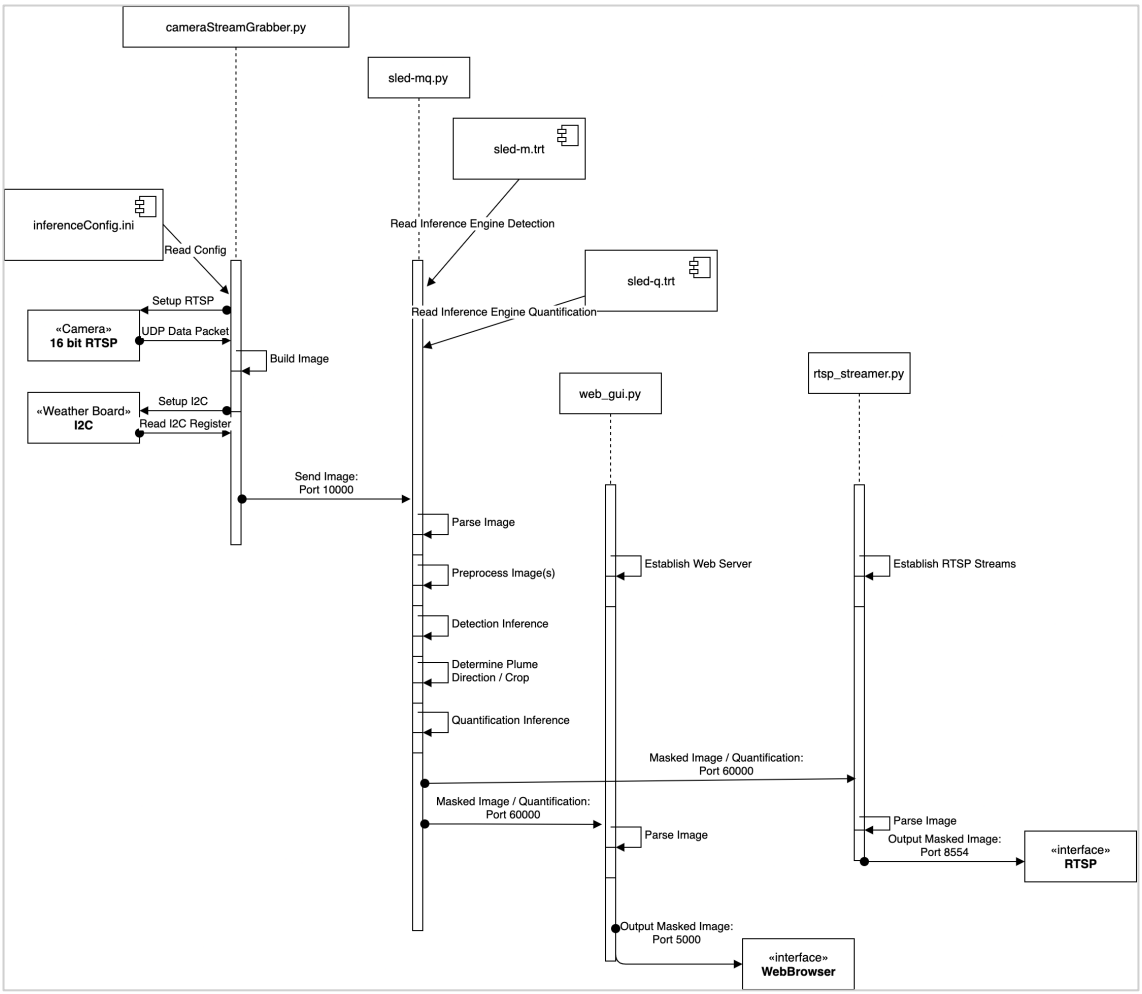

Figure 2. SLED/Q Software Diagram

Table 3. SLED/Q Source Tree

File/Directory Name	Type	Description
README.md	file	Readme and instruction file for the codebase
python_infer/SLED-MQ.sh	file	Primary execution script for the SLED/MQ program that wraps all arguments in a Bash shell script
python_infer/inferenceConfig.ini	file	Configuration file with options and definitions for the SLED/MQ program
python_infer/infer_preprocessors.pyc	file	SLED/MQ preprocessor definitions
python_infer/sled-m.pyc	file	SLED/M inference engine compiled binary
python_infer/sled-mq.pyc	file	SLED/MQ inference engine compiled binary
python_infer/models/	directory	Folder for SLED/MQ inference engines
python_infer/models/sled-m.trt	file	contains a SLED/M inference engines compiled binary
python_infer/models/sled-q.trt	file	contains a SLED/Q inference engines compiled binary
python_infer/Flask_Server/	directory	Folder for Web Viewer and Control server
python_infer/Flask_Server/web_gui.pyc	file	Web Viewer and Control server for SLED/MQ
python_infer/cameraStreamGrabber.pyc	file	Configurable input streaming utility and camera driver
python_infer/g300aLiveFrameGrabber.pyc	file	FLIR g300a driver module
python_infer/rtsp_streamer.pyc	file	RTSP Streaming output for SLED/M
python_infer/weatherboard/	directory	Folder for Weather Module Interfacing
python_infer/weatherboard/BME280.pyc	file	Interface with BME280 weather module
python_infer/weatherboard/SI1132.pyc	file	Interface with SI1132 weather module
python_infer/weatherboard/weatherBoardLive.pyc	file	Concatenate weather data from modules for preprocessor definitions

2.4 Compilation and Execution Instructions

This section describes how to compile and run SLED/Q.

2.4.1 Compilation

Python source code requires no compilation.

2.4.2 Execution

The two methods of running inference using the SLED/MQ software are described in sections 2.4.2.1 and 2.4.2.2.

Streaming Configuration

1. Bash Script
    a. Usage: SLED-MQ.sh --<streaming_mode>
    b. The available streaming modes are listed below
        i. --web → Outputs the stream via Web graphical user interface (GUI)
        ii. --rtsp → Outputs the stream via RTSP streamer

2.4.2.1 Option 1: Web GUI and Control

Works best on Google Chrome. Works on Firefox with slight bugs. Not working on Safari.

Connect to the Web Server

1. Run the SLED-MQ.sh file located in python_inference/SLED-MQ.sh directory with the --web or -w flag.
    a. Server is ready when you see: * Running on http://0.0.0.0:5000/ (Press CTRL+C to quit)
2. In a web browser, connect to the IP address of the Jetson port 5000.
3. The GUI should be visible as shown in Figure 3.

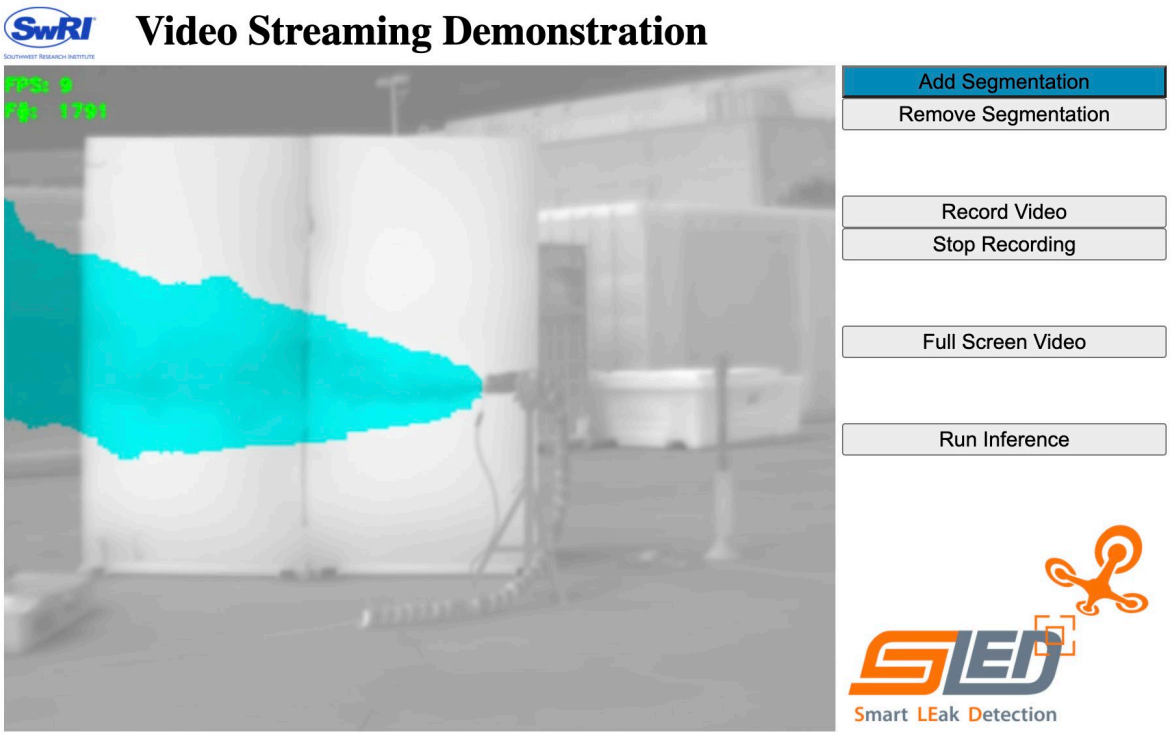

Figure 3. SLED/Q Web GUI

To Run the Inference Script

1. Press the button labeled "Run Inference". It takes about 25 seconds for an output to appear.

Settings Adjustments

2. In the python_infer directory there is a Configuration file called inferenceConfig.ini. This contains all the possible settings that can be varied for inference. These settings need to be changed BEFORE running the GUI; changing them after will result in usage of the old settings. A detailed description of the different settings and how they function is seen in Table 4.

Table 4. SLED/Q Runtime Options

Section	Parameter	Options	Default Value	Function
generatorOpts	distance	Integer distance in feet the camera is from the methane plume	30	This tells the algorithm how far the camera is from the plume so that it can scale the frames appropriately before running inference

Section	Parameter	Options	Default Value	Function
modelOpts	quant_model_path	Path to SLED/Q inference engine compiled binary	./models/sled-q.trt	Provides the algorithm with the location of the methane quantification model
	detect_model_path	Path to SLED/M inference engine compiled binary	./models/sled-m.trt	Provides the algorithm with the location of the methane detection model
inferenceOpts	g300a_serverport	Port number to the g300a camera	1234 - needs to be provided by user	The port number provided here allows for communication with the camera when in 'live' mode

To Save Video Feed

1. Press the button labeled "Record Video." This will create a file in the directory from where the program was run on the jetson labeled outpy#-YEAR_MONTH_DAY_HOURMINUTESECOND.avi
2. To stop recording, press the button labeled "Stop Recording"
    a. The video that is recorded is exactly what is seen in the frame. If segmentation is on, then it will appear in the recording. If segmentation is off it will not appear.

2.4.2.2 Option 2: RSTP

1. Run the SLED-MQ.sh file located in python_inference/SLED-MQ.sh directory with the --rtsp or -r flag.
2. Connect Via Media player; VLC works great. There will be two streams, one for just the raw output, another with the mask overlay. Change IP to current system IP address. Output shown in Figure 4.
    a. rtsp://{IP}:8554/sled
    b. rtsp://{IP}:8554/raw

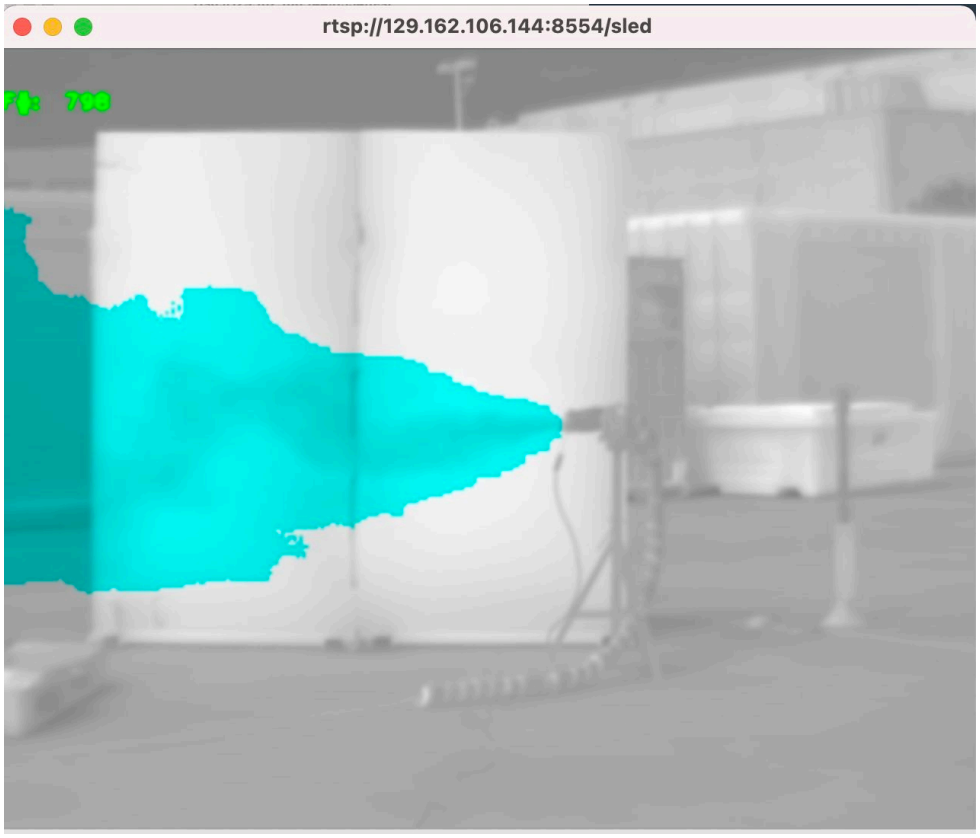

Figure 4. SLED/Q RTSP Output

2.5 Software Version

The SLED/Q version being delivered via this document is v4.0, created on 09/30/2021. The source set used for this baseline is attached in Appendix A.

Prior to this version, baselines were created as development of beta testing progressed. A history of baselines, along with the baseline being delivered (last entry), is shown in Table 5.

Table 5. Software Version History

Version	SVN Tag	Description
0.1	2017_0621_1056_SLED/M	Initial baseline that compiles. Not a functional build, but proves linking of (1) camera driver, (2) background subtraction libraries, (3) data loading libraries, (4) OpenCV, and (5) Caffe.
0.2	2017_0629_1042_SLED/M	First build to successfully display an image from both the FLIR A6604 and FLIR A65 camera.
0.3	2017_0711_1025_SLED/M	First build to successfully show an image from the camera, run it through background subtraction, and show the resulting foreground extraction.

Version	SVN Tag	Description
0.4	2017_0713_1646_SLED/M	First known build to reliably load a camera configuration file and display GUI debug output and a valid foreground measure using FLIR A65.
0.5	2017_0714_1145_SLED/M	First build to reliably work with both cameras (FLIR A6604 and FLIR A65), loading configuration files as they are modified (minimal hard coding), and exit gracefully upon camera shutdown or loss of network.
0.6	2017_0724_0933_SLED/M	First build to multi-thread the simulated reading of files, the camera feeds, the web interface, and the GUI display thread. The web server thread and the processing thread appear to be initially correctly operating; however, Open CV displays are not yet working in parallel with Qt.
0.7	2017_0725_1042_SLED/M	First build to reliably not have conflicts between Qt and Open CV imshow() calls (via the enable_debug_gui flag). Shown to successfully display images in Open CV and the web server with all three input sources: simulated data, FLIR A65 data, and FLIR A6604 data.
0.8	2017_0802_1344_SLED/M	This version successfully displays the user output webpage (if it displays the raw feed and bg subtracted image) from simulated data and FLIR A6604. Caffe Classifier loads and runs successfully for simulated (if commented in) but commented out due to it crashing when connected to real camera.
0.9	2017_0808_1554_SLED/M	This version successfully ingests feeds, classifies them against the configured Caffe model, and runs the web server for user output. First known release with no known major issues (although minor issues do exist).
1.0	2017_0814_1618_SLED/M	This is the first version that successfully uses the best-known model to overlay a methane detection on data used for validation and displays minimal false positives in ambient conditions.
1.1	2017_0822_1620_SLED/M	Added program option to decimate simulated data. Modified logo to have DOE/NETL/SwRI (along with SLED). Added white text box around image filenames/timestamps for much easier reading. Added Initializing box to classified image while BG model being generated. Fixes issue with classifier and raw image not keeping up on web display.

Version	SVN Tag	Description
1.2	2017_0828_1438_SLED/M	Fixes bug with Caffe net (image_queue_) not being correctly populated (major issue), updated CLAHE for 16-bit scaling with Open CV3 (better web browser viewing), fixes HTTP streaming lag issue, ensures Caffe cleanly shuts down.
1.3	2017_0908_0854_SLED/M	Addresses issue with RemoveDeadPixels() incorrectly modifying images. Adds a simple fault system for camera disconnect and low space (and associated GUI updates). Modifies classified image to include probability coloring (red = high, blue = low). Cleaner shutdown on both Tegra and deep-cruncher via Ctrl-C.
1.4	2017_0914_1550_SLED/M	Code cleanup, additional comments. Prototype of methane detection sensitivity included. Adds security to HTTP server code. Fixes CDT/UTC issue with BG model filename. Additional checks on ensuring program can write to output directory. Added --exit_after_bg_gen functionality. Check in Caffe model as part of SLED/M repository.
2.0	2018_0920_0216_SLED/M	Added final tag. Updated charts with final software design. Updated software dependencies table. Updated class definitions.
3.0	2019_1113_1536_SLED/M	Added Tag for Aerial Detection Network.
3.1	2020_0311_1230_SLED/M	Updating Tag to include web-based user interface for usability.
4.0	2021_0930_1400_SLED/MQ	Added Quantification Capabilities

3. MECHANICAL OVERVIEW

The hardware required to operate the Smart Leak Quantification Algorithm is listed below:

1. MWIR OGI Camera
    a. The current software has only been tested on 16-bit RTSP camera interface
2. ODROID Weatherboard 2 weather module
3. Nvidia Tegra TX-2 or NVIDIA Xavier AGX or similar Linux based computer
4. Locally attached Display or Ethernet or Wi-Fi enabled device to view the output of the system

The hardware wiring is shown in Figure 5.

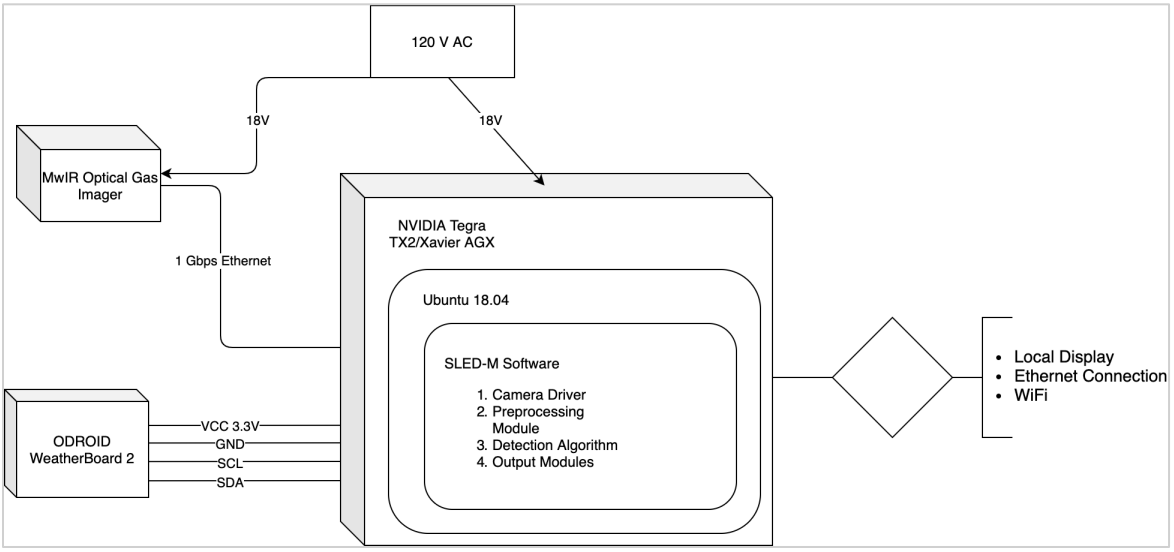

Figure 5. SLED/Q Hardware Diagram

4. TEST OVERVIEW AND RESULTS

Our best performing quantification model was able to achieve the following metrics on valid frames where 1) the methane was detected and 2) a valid ΔT was observed. These results are shown in Figure 6 and Figure 7.

1. Average Percentage Prediction Error: 12.3%
2. Accuracy ±50scfh: 97.78%

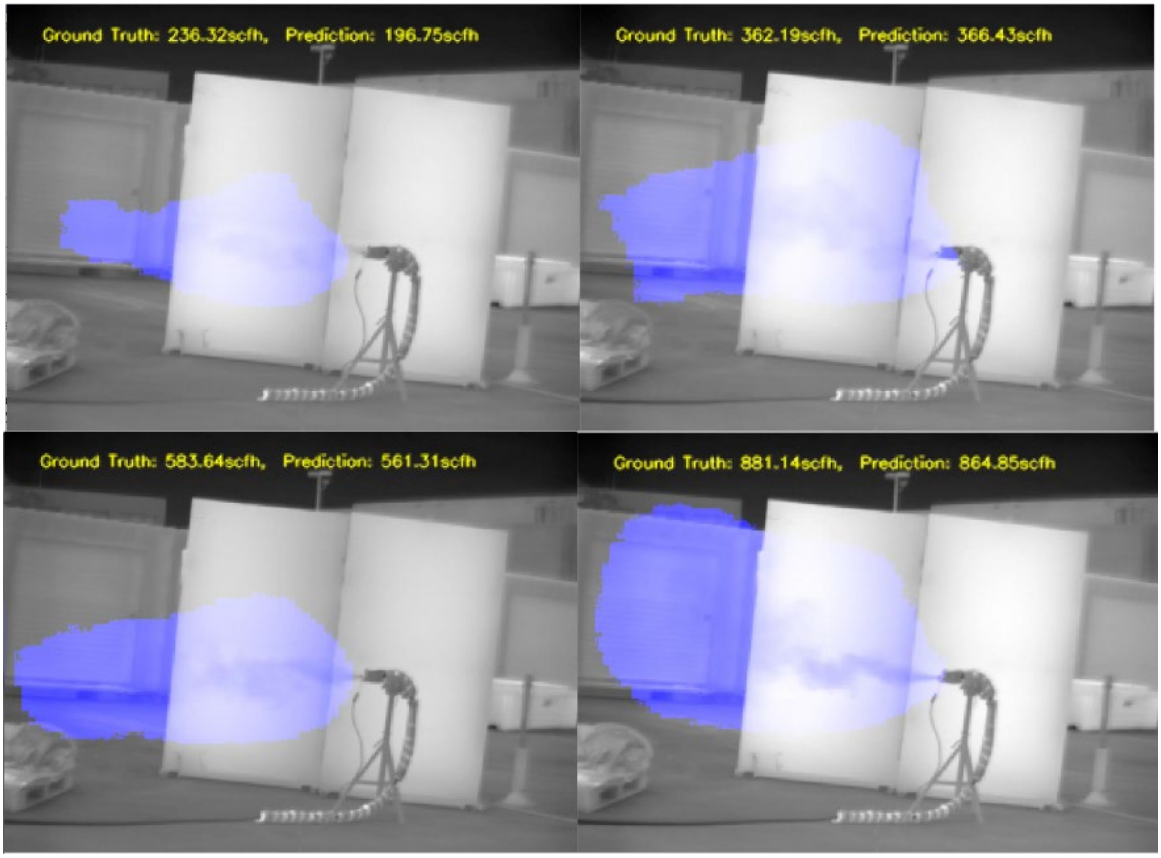

Figure 6. Detection and Quantification at Multiple Flowrates

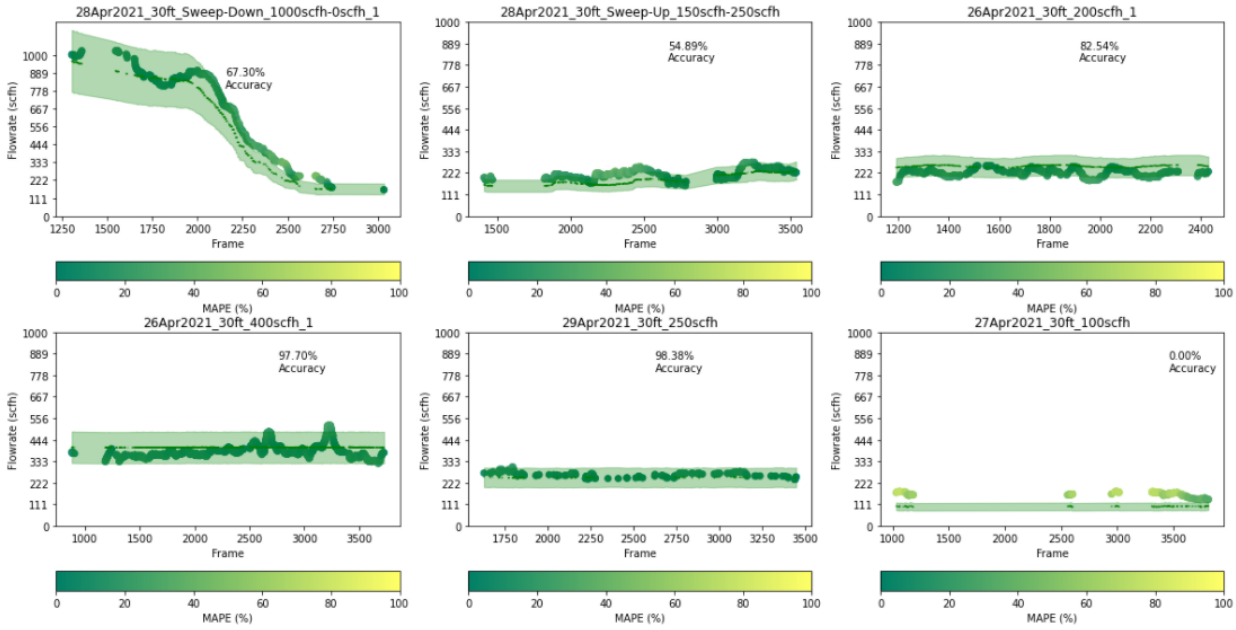

Figure 7. SLED/Q Benchmark Metrics

4.1 System Benchmarks

The provided code timings and benchmarks are shown in Table 6.

Table 6. System Performance Benchmarks

	Model	Precision	Input Size	Frames Per Second
Xavier AGX	Detection	FP16	240x320x5	30.82 FPS
	Quantification	FP16	240x320x1	

5. CONCLUSION

SLED/Q has the ability to autonomously detect fugitive methane emissions, deployable on a drone for remote inspection and faster more reliable site inspections as well as the ability to quantify detected plumes in one tool while keeping operators out of hazardous areas. This technology can meet some customer needs including an increase in speed of periodic pipeline inspection, by augmenting visual inspection for the operator, allowing them to focus on safety and other cost and risk reductions.

SLED/Q can detect methane leaks as low as three (3) scfh, with a precision of 96.6% and false positive rate of 2.22%. Additionally, SLED/Q is capable of estimating methane flow rate and concentration within 12% of ground truth flow rate. The technology itself only requires the MWIR OGI camera providing SLED/Q with a flexible competitive advantage and reducing the need on the customer to use additional instrumentation and equipment.

Appendix A SLED/Q Software

Please see SLED-Q.zip